INDIRECT FEEDBACK KALMAN FILTER BASED SENSOR FUSION FOR REDUCING NAVIGATION ERRORS OF AN AUTONOMOUS WHEELCHAIR

SOH YING WEI

MASTER OF ENGINEERING AND SCIENCE

LEE KONG CHIAN FACULTY OF
ENGINEERING AND SCIENCE
UNIVERSITI TUNKU ABDUL RAHMAN
DEC 2018

INDIRECT FEEDBACK KALMAN FILTER BASED SENSOR FUSION FOR REDUCING NAVIGATION ERRORS OF AN AUTONOMOUS WHEELCHAIR

By

SOH YING WEI

A dissertation submitted to the
Department of Mechatronics and Biomedical Engineering,
Lee Kong Chian Faculty of Engineering and Science,
Universiti Tunku Abdul Rahman,
in partial fulfillment of the requirements for the degree of
Master of Engineering and Science
December 2018

ABSTRACT

INDIRECT FEEDBACK KALMAN FILTER BASED SENSOR FUSION FOR REDUCING NAVIGATION ERRORS OF AN AUTONOMOUS WHEELCHAIR

Soh Ying Wei

Patients with severe motor disabilities have difficulty maneuvering a wheelchair. An autonomous wheelchair with facility for destination selection via a brain-computer interface or eye tracker would be a possible solution. Accurate localization is important for such an autonomous wheelchair. Normally relative localization of the wheelchair is carried out using an odometry method based on data from the wheel encoders. The current study aims to reduce wheelchair navigation errors in an indoor environment by the introduction of an additional sensor - a gyroscope. Fusion of the wheel encoders and gyroscope was effected using indirect feedback Kalman filter algorithm. The algorithm was programmed in a small memory microcontroller to increase the portability of the wheelchair. The results of the study showed that fusion of encoders and gyroscope using indirect feedback Kalman filter significantly improved the wheelchair navigation accuracy (as high as 7.8 folds) in terms of mean distance errors compared to using odometry.

ACKNOWLEDGMENT

I would like to express my utmost gratitude and appreciation to several individuals whom had extended their assistance in the process of completing this study. I am very thankful to my supervisor Prof Dato Dr Goh Sing Yau and co-supervisor Dr Mok Siew Ying for their relentless guidance, support and encouragement that enables me to develop a good research, writing and presentation skills. I am grateful to Mr Danny Ng Wee Kiat invaluable guidance in firmware, electronics and Kalman filter.

Special thanks to the entire UTAR flagship project team, Mr Ho Chan Cheong, Mr Huong Guo Fu and my fellow UTAR friends for their expertise, kind assistance and support throughout the entire research. Last but not least, I would like to thank my family for their continuous support.

APPROVAL SHEET

This dissertation entitled "**INDIRECT FEEDBACK KALMAN FILTER BASED SENSOR FUSION FOR REDUCING NAVIGATION ERRORS OF AN AUTONOMOUS WHEELCHAIR "** was prepared by SOH YING WEI and submitted as partial fulfillment of the requirements for the degree of Master of Engineering and Science at Universiti Tunku Abdul Rahman.

Approved by:

_____

(Prof. Dato' Ir Dr. GOH SING YAU) Date:
Supervisor
Department of Mechanical and Material Engineering
Lee Kong Chian Faculty of Engineering and Science
Universiti Tunku Abdul Rahman

_____

(Dr. MOK SIEW YING) Date:
Co-supervisor
Department of Mechatronics and Biomedical Engineering
Lee Kong Chian Faculty of Engineering and Science
Universiti Tunku Abdul Rahman

LEE KONG CHIAN FACULTY OF ENGINEERING AND SCIENCE

UNIVERSITI TUNKU ABDUL RAHMAN

Date: _____

SUBMISSION OF DISSERTATION

It is hereby certified that **SOH YING WEI** (ID No: **14UEM06778**) has completed this dissertation entitled "**INDIRECT FEEDBACK KALMAN FILTER BASED SENSOR FUSION FOR REDUCING NAVIGATION ERRORS OF AN AUTONOMOUS WHEELCHAIR"** under the supervision of **Prof. Dato' Ir. Dr. GOH SING YAU** (Supervisor) from the Department of Mechanical and Material Engineering, Lee Kong Chian Faculty of Engineering and Science, and **Dr. MOK SIEW YING** (Co-Supervisor) from the Department of Mechatronics and Biomedical Engineering, Lee Kong Chian Faculty of Engineering and Science.

I understand that University will upload softcopy of my dissertation in pdf format into UTAR Institutional Repository, which may be made accessible to UTAR community and public.

Yours truly,

_____

(SOH YING WEI)

DECLARATION

I hereby declare that the dissertation is based on my original work except for quotations and citations which have been duly acknowledged. I also declare that it has not been previously or concurrently submitted for any other degree at UTAR or other institutions.

Name _____

Date _____

TABLE OF CONTENTS

LIST OF TABLES

LIST OF FIGURES

LIST OF ABBREVIATION

BCI	Brain Computer Interface
CCW	Counter clockwise
CW	Clockwise
EKF	Extended Kalman Filter
GPS	Global Positioning System
IMU	Inertial Measurement Unit
KF	Kalman Filter
LiDAR	Light Detection and Ranging
PF	Particle Filter
UKF	Unscented Kalman Filter

CHAPTER 1

INTRODUCTION

Conventional wheelchair was one of the most common assistive tools for mobility impaired people (Cavanini et al., 2017). In the recent years, the conventional wheelchair is transformed into a smart wheelchair by integration of electronic systems. Autonomous navigation is one of the important tasks in a smart wheelchair (Utaminingrum et al., 2017). The essential part of a wheelchair navigation system is localization that determines the wheelchair position and orientation (Cavanini et al., 2017).

Localization of mobile robots is categorized into two main groups which are relative localization and global localization (González and Rodriguez, 2009; Zhou and Huang, 2011). Most previous studies used global localization to correct relative localization which caused less attentions directed towards improvement of relative localization (Lv et al., 2017; Choi et al., 2011; D'Alfonso et al., 2015; Marín et al., 2013).

The current study focuses on improvement of relative localization of the wheelchair. Odometry is a relative localization method of estimating the robot current position and orientation relative to a known origin by using the wheel encoder information. An assumption is made where wheel rotations could be translated into linear motions on the floor (Chong and Kleeman, 1997; Zaki et al., 2014; Seongwoo Jang et al., 2015).

However, odometry is subject to systematic errors and non-systematic errors. Systematic errors are mainly due to the imperfection in the design or mechanical implementation of the wheelchair. For example, misalignment of wheels, uncertainty of wheelbase and unequal wheel diameters. They are vehicle-specific and remain consistent over a run. Non–systematic errors are caused by wheelchair interaction with the unpredictable surface conditions such as irregular floor surface, unforeseen objects on the floor and wheel slippage (Borenstein and Feng, 1996; Guran et al., 2015; Goronzy and Hellbrueck, 2017; Ruan et al., 2012; Dang et al., 2016) .

On smooth surfaces, systematic errors are greater than non-systematic errors. On rough surfaces the non-systematic errors may be dominant due to the significant irregularities of the floor surface (Abbas et al., 2006; Borenstein and Feng, 1996). The present study focuses on reducing the systematic errors since the wheelchair is intended to be used on smooth surfaces.

The two most dominant sources of systematic errors are uncertainties of the wheelbase, E_b and unequal wheel diameters, E_d .Wheelbase is the distance between two drive wheels of differential drive robot contact point with the floor. The wheelbase uncertainty arises as the rubber tires contact the floor in a contact area instead of a point. Unequal wheel diameters are caused by the inability of manufacturers to produce tires with exactly the same diameter and asymmetric load distribution of robots that compresses the

rubber tires differently (Borenstein and Feng, 1996; Chivarov et al., 2015; Xuying et al., 2017; Panich and Afzulpurkar, 2011).

Other than systematic and non-systematic errors, the odometry equations also contribute to navigation errors. This is due to the assumption made in odometry where arbitrary motion is approximated by using a set of short straight-line segments (Borenstein and Feng, 1996).

The objective of this study is to reduce wheelchair navigation errors which include wheelbase error and errors caused by unequal wheel diameters by introducing an additional sensor – a gyroscope. Fusion of the data from the wheel encoder and gyroscope was implemented using indirect feedback Kalman filter. The wheelchair system was equipped with two rotary encoders and one gyroscope sensor. It was programmed to travel in a square path. The indirect feedback Kalman filter algorithm was implemented into the wheelchair navigation system by using a microcontroller.

The rest of the dissertation is arranged as below:

Chapter 2 consists of the literature review on relative and global localization, overview of navigation systems developed by other researchers and sensor fusion methods.

Chapter 3 describes the mathematical model used, experiment setup and procedures.

Chapter 4 presents the results and discussion of bidirectional square path experiments.

Chapter 5 concludes the dissertation with the findings of this study and suggestions for future work.

CHAPTER 2

LITERATURE REVIEW

2.1 Relative localization and global localization

For relative localization, the position and orientation of robots are determined relative to an initial position. The position coordinates are calculated based on the data that is obtained from the onboard sensors such as gyroscopes, encoders and accelerometers (González and Rodriguez, 2009; Zhou and Huang, 2011; Huang et al., 2015; Kundu et al., 2017). The commonly used relative localization methods are odometry and dead reckoning. Odometry uses only wheel encoders for localization whereas dead reckoning uses inertial measurement units (IMU) such as gyroscope and accelerometers (González and Rodriguez, 2009; Tai et al., 2014; Peter et al., 2016; Lobo et al., 2014). Some of the advantages of relative localization include simplicity, low cost of application, low illumination, not dependent on global localization sensors and relative ease in estimating position in real time compared to global localization (Zaki et al., 2014; Lv et al., 2017; Cho et al., 2011). However, it is susceptible to accumulation of positioning errors over time and distance travelled (Péter et al., 2016; Zhong et al., 2017).

For global localization, the position and orientation of robot are calculated based on a global reference frame (Leonard and Durrant-Whyte, 1991; González and Rodriguez, 2009; Huang et al., 2015; Kundu et al., 2017). The information is obtained from landmarks, beacons or satellite-based signals

that are detected from vision and light detection and ranging (LiDAR) sensors (Goel et al., 1999; Huang et al., 2015; Baatar et al., 2014; Nazemzadeh et al., 2017; Kundu et al., 2017). LiDAR sensors produce high accuracy of robot estimation (from few centimeters to tens of meters). The position and orientation of the robot are estimated externally from the beacons or landmarks placed in the environment without accumulation of positioning errors (Goel et al., 1999; Nazemzadeh et al., 2017; Zhong et al., 2017).The main disadvantages of global localization, however, are that the sensors and landmarks are very costly, difficult to install and maintain and possible signal interference due to mirror reflection (Lee, 2015; Nazemzadeh et al., 2017; Lee et al., 2015; Yang and Wang, 2011).

The current system is developed as part of an autonomous BCI wheelchair project (Ng et al., 2014). In the BCI wheelchair, both relative localization and global localization are implemented. The wheelchair has an alternative to navigate by using relative localization in areas where beacons are not available for the wheelchair to perform global localization.

2.2 Overview of navigation systems developed by other researchers

Table 2.1: Overview of different navigation systems.

Authors	Types of Sensor Used	Sensor Fusion Method	Method of Implementation
(Al Khatib et al., 2015)	Encoder, compass, gyroscope, accelerometer and global positioning system (GPS)	Extended Kalman Filter	Performed simulation on a mobile robot
(Seongwoo Jang et al., 2015)	Encoder and 2D laser range finder	Particle filter	Performed simulation on AGV
(Yoon et al., 2015)	Encoder and Stargazer (position sensor for an image recognition device)	Kalman filter	Performed simulation on a mecanum wheeled automated guided vehicle (AGV)
(Jeon et al., 2016)	Encoder and magnetic sensor	Unscented Kalman Filter	Performed simulation on an autonomous vehicle
(Nasir and Roth, 2012)	Encoder, gyroscope, magnetometer and electronic compass	Kalman filter and Extended Kalman filter	Performed experiment on a two wheel differential drive robot by using a remote computer to implement sensor fusion algorithm
(Lv et al., 2017)	Encoder, gyroscope and magnetometer	Self-tuning Kalman filter	Performed experiment on a skid-steering robot by using computer to implement sensor fusion algorithm
(Wardana et al., 2013)	Encoder and vision system	Particle filter	Performed experiment on an electric wheelchair by implementing sensor fusion algorithm in the microcontroller

As shown in Table 2.1, most of the previous researchers implemented the sensor fusion algorithm either by simulation or experiment using computer. There was only one study where the sensor fusion algorithm was implemented

in a microcontroller (Wardana et al., 2013). The current study proposed implementation of sensor fusion of encoder and gyroscope in the microcontroller to increase the portability of the wheelchair.

2.3 Sensor Fusion Methods

Kalman filter, Extended Kalman filter (EKF) (Al Khatib et al., 2015; Lynen et al., 2013), Unscented Kalman filter (UKF) (Jeon et al., 2016; Anjum et al., 2010) and Particle filter (PF) (Won et al., 2014; Jaros et al., 2017) are the commonly used sensor fusion methods. Kalman filter is applied in the linear system whereas EKF, UKF and PF are used in the non-linear system.

2.3.1 Kalman filter

Kalman filter is an optimal estimator of current variable state based on the understanding of the system model, device measurement output, system noise, measurement noise and dynamic model uncertainties. The data is processed in a recursive way where the current estimate is calculated by using the previous calculated estimate and the current input measurement. Thus, it does not require the information of past data (Maybeck, 1979). Kalman filter is only applicable in the linear system where the process and measurement errors are modeled as white Gaussian noises (Luo and Chang, 2012; Pelka and Hellbrück, 2016; Fung et al., 2017). The state space model of Kalman filter is written as

$$x_k = F_k x_{k-1} + B_k u_k + w_k \quad (2.1)$$

$$z_k = H_k x_k + v_k \quad (2.2)$$

where x_k is the state vector, F_k is the state transition matrix, B_k is the control input matrix, u_k is the control input, z_k is the measurement vector, H_k is the measurement matrix, w_k and v_k are the zero mean white Gaussian process noise and measurement noise with covariance matrix Q_k and R_k.

Kalman filter estimation by using efficient matrix operations has led to its high computational efficiency (Luo and Chang, 2012). Kalman Filter is easy to implement as the calculations are mostly in linear form except for the matrix inversion (Umamageswari et al., 2012). It has a computational complexity of *O(N)* with N as the number of state variables (Luo and Chang, 2012;Paliwal and Basu, 1987;Pelka and Hellbrück, 2016).

2.3.2 Extended Kalman filter

The system model and measurement model of EKF are represented by the following equations:

$$x_k = f(x_{k-1}, u_k) + w_k \quad (2.3)$$

$$z_k = h(x_k) + v_k \quad (2.4)$$

The EKF equations are similar to Eq. (2.1) and Eq. (2.2) in Kalman filter where u_k is the control input. However, the system is no longer linear due to the non-linear functions f and h in the system and measurement

models. The system noise, w_k and measurement noise v_k are zero-mean Gaussian noise with covariance Q_k and R_k respectively as shown below (Kumari et al., 2015; Fang et al., 2018):

$$w_k \sim N(0, Q_k) \tag{2.5}$$

$$v_k \sim N(0, R_k) \tag{2.6}$$

The EKF works in a two-stage process which is prediction and update similar to KF. It estimates the state estimate, $\hat{x}_{k|k-1}$ and covariance, $P_{k|k-1}$ in the prediction state. In the following equations, the $\hat{\mathbf{x}}_{m|n}$ denotes the estimate of **x** at time *m* given observations up to and including at time $n \leq m$ where k > 0.

$$\hat{x}_{k|k-1} = f(\hat{x}_{k-1|k-1}, u_k) \tag{2.7}$$

$$P_{k|k-1} = F_k P_{k-1|k-1} F_k^T + Q_k \tag{2.8}$$

For the update process, matrix F and H are computed in terms of Jacobian as follows:

$$F_k = \left.\frac{\delta f}{\delta x}\right|_{\hat{x}_{k-1|k-1}, u_k} \qquad H_k = \left.\frac{\delta h}{\delta x}\right|_{\hat{x}_{k-1|k-1}, u_k} \tag{2.9}$$

The second and higher order terms in the Taylor series expansion are assumed to be negligible in the EKF linearization process. The main advantage of EKF is that it is straightforward and easy to use (Luo and Chang, 2012; Borsje et al., 2005). However, the linearization process can cause instability (Borsje et al., 2005). The EKF computational complexity is $O(N^3)$ with N as the number of state variables (Pelka and Hellbrück, 2016).

2.3.3 Particle filter

Particle filter was introduced by Gordon et al., 1993 based on the Sequential Monte Carlos method (Crisan and Doucet, 2002; Fung et al., 2017; Feng et al., 2015). It is able to represent arbitrary probability density functions including non-linear system and non-Gaussian distribution. The filter works by using a set of N random samples which are known as particles, $\left\{x_k^{(i)}\right\}_{i=1}^{N}$ with their associated weights, $\left\{w_{k|k-1}^{(i)}\right\}_{i=1}^{N}$ to approximate the probability density function, $p(x_k|y_{1:k-1})$.

The weights are called importance weight with $\sum_{i=1}^{n} w_k = 1$ .The equation is shown below:

$$p(x_k|y_{1:k-1}) \approx \sum_{i=1}^{N} w_{k|k-1}^{(i)} \delta(x_k - x_k^{(i)}) \tag{2.10}$$

The likelihood of measurement is used to update the particle weights. For new iterations, the particles are resampled by producing new particles at points with the largest weight. The lower-weight particles are removed. This step prevents the filter from diverging (Gordon et al., 1993; Fung et al., 2017; Uddin et al., 2017).

PF requires a large amount of particles to estimate the posteriori distribution which increases the computational complexity and time (Won et al., 2014; Pelka and Hellbrück, 2016). When the number of particles is

reduced, it might not reflect the true state of the distribution and the particle filter diverged (Pelka and Hellbrück, 2016).

2.3.4 Unscented Kalman filter

Unscented Kalman filter (UKF) is another type of recursive filter and is restricted to Gaussian distribution as EKF. The difference between UKF and EKF is on how they linearized non-linearities. It makes approximation of non-linearities without Taylor series expansion. Instead of approximation of non-linearities, the filter uses sample points which are sampled through non-linear models and remodeled after sampling. The distribution is represented by individual sample points as shown below (Pelka and Hellbrück, 2016; Ericsson and Eriksson, 2014; Fang et al., 2018):

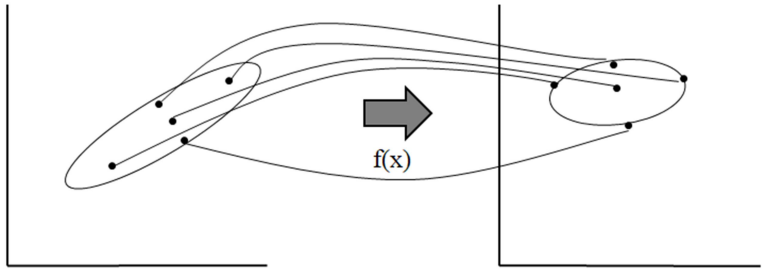

Figure 2.1: Sigma points of a Gaussian distribution that were propagated via a non-linear function, f(x) (Pelka and Hellbrück, 2016)

UKF estimated a posterior distribution by using sigma points where Jacobian matrix calculation is not needed. The UKF computational complexity is almost similar to first order EKF $O(N^3)$ (Pelka and Hellbrück, 2016; Fang et al., 2018; Julier and Uhlmann, 2004).

2.3.5 Summary of different sensor fusion methods

Table 2.2: Summary of different sensor fusion methods.

Method	Advantages	Disadvantages
Kalman Filter	• Computational efficiency is high • Ease of implementation • Low computational complexity	• Assumptions limited to linear and Gaussian distribution
Extended Kalman Filter	• Applicable to non-linear system • Computational efficient in dynamic state estimation	• Not usable for non-Gaussian process noise • High computational complexity • Linearization process can cause filter instability
Unscented Kalman Filter	• Applicable up to third order non-linear system • Linearization of state and covariance is not required	• Computational complexity is almost the same as first order EKF
Particle Filter	• Able to represent arbitrary probability densities • Applicable in non-linear or non-Gaussian system	• High computational complexity • Degeneracy of particles due to inappropriate resampling • High number of particles is required

Based on the comparison of all the sensor fusion methods (Table 2.2), Kalman filter was chosen. This is due to its ease of implementation, high computational efficiency and simplicity of the linear model which reduced the computational complexity. Therefore, Kalman filter is suitable for implementation in a small memory microcontroller.

2.3.6 Direct Kalman filter and indirect Kalman filter

There are two main formulations of Kalman filter for error compensation in the navigation systems, namely direct Kalman filter and indirect Kalman filter.

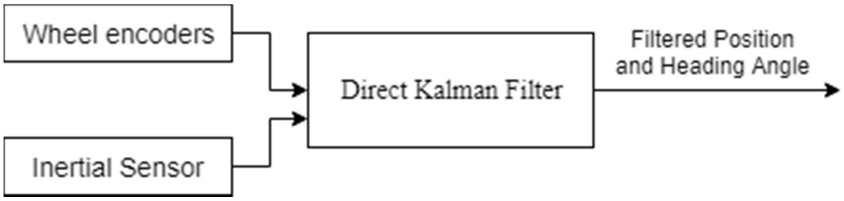

Figure 2.2: Direct Kalman filter.

Direct Kalman filter modeled the total state representation that incorporated dynamic model of the system. The state variables of the system such as position and heading angle were estimated (Figure 2.2). The measurements were the encoder output and inertial sensor output (Sheijani et al., 2013; Park et al., 1996; González and Rodriguez, 2009). The advantage of this configuration is that it provides significant performance improvement because the Kalman gain is updated continually as opposed to fixed gain in classical approach (Park et al., 1996; González and Rodriguez, 2009). However, the filter is run in the navigation loop -- if the Kalman filter fails, the whole navigation system fails (Sheijani et al., 2013; Park et al., 1996; González and Rodriguez, 2009).

Indirect Kalman filter modeled the error state of the system. The error state variables of the system such as position error and heading angle error were estimated. The measurement was the difference between the encoder

output and inertial sensor output. This formulation enabled the navigation system to continue with its operation even if the filter fails. This was because the calculated position and heading angles could still be obtained from the encoder navigation system as the filter was placed outside of the navigation loop. The disadvantage of this filter, however, is that the real state variables of the navigation system were not estimated (Park et al., 1996; González and Rodriguez, 2009).

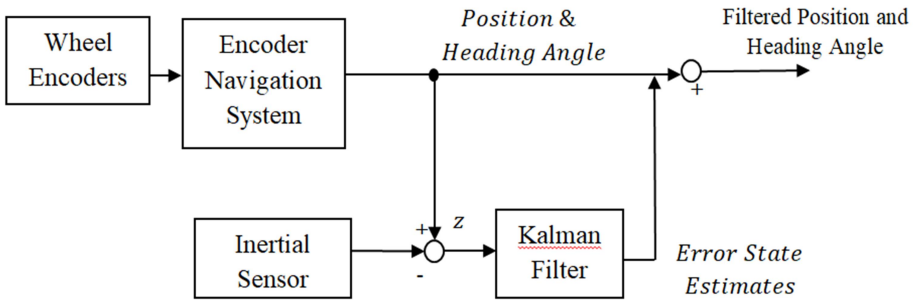

Figure 2.3: Indirect feedforward Kalman filter.

Indirect Kalman filter is implemented in two ways namely feedforward and feedbackward (Park et al., 1996; González and Rodriguez, 2009; Li et al., 2016). For feedforward structure, the Kalman filter estimated the error variables. These error estimates would be used to compensate the encoder navigation output which is shown in Figure 2.3. The drawback of this structure is that the navigation errors would grow over time as the error estimates were not fedback into the encoder navigation system.

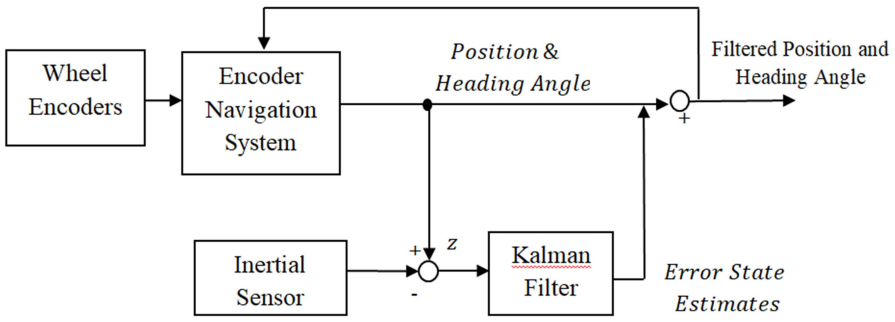

Figure 2.4: Indirect feedback Kalman filter.

Feedback structure implementation was similar to feedforward structure where the Kalman filter estimated the error variables. The main difference was error estimates were fedback into the encoder navigation system to correct the encoder navigation system output (Figure 2.4). Therefore, it overcame the drawback of feedforward structure by keeping the navigation errors small (Park et al., 1996; González and Rodriguez, 2009; Li et al., 2016). Indirect Kalman filter was widely used in robot, vehicle, underwater and attitude and heading reference navigation system (Park et al., 1996; Chung et al., 2001; Sheijani et al., 2013; Hou et al., 2011; Li et al., 2016; Chang et al., 2017).

In this study, indirect feedback Kalman filter was used to integrate the outputs from the wheel encoder and the gyroscope in order to provide a more accurate estimate of the X-Y position and the heading angle, θ, of a differential drive wheelchair. Indirect feedback Kalman filter was applied in the wheelchair navigation system because the design difficulty was reduced by using a linear error model (Hou et al., 2011). Another advantage of indirect

feedback Kalman filter is that the wheelchair navigation filter would not fail even if the filter failed due the divergence of error covariance (Park *et al.*, 1996; Sheijani *et al.*, 2013). This is because the wheelchair could still navigate by using the unfiltered position and heading angle which lacked the correction provided by the filter.

CHAPTER 3

METHODOLOGY

3.1 Mathematical models

3.1.1 Overview

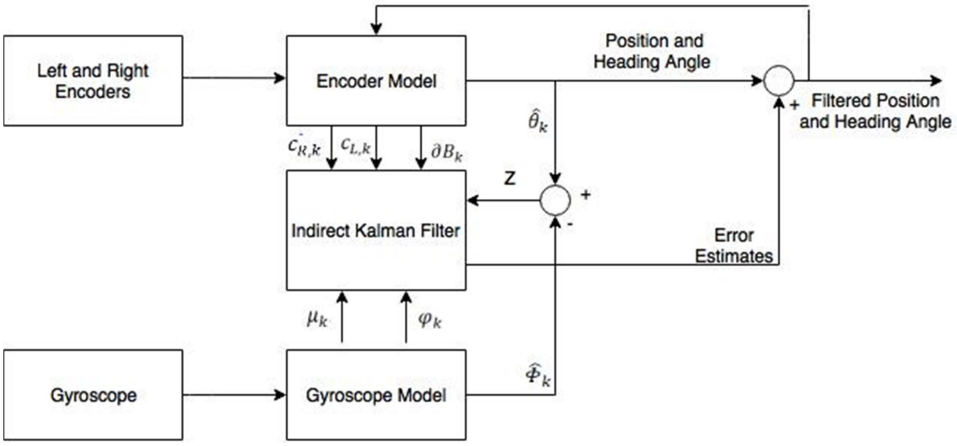

Figure 3.1: Overview of the wheelchair navigation system.

Figure 3.1 shows the overview of the wheelchair navigation system. The indirect feedback Kalman filter estimated the error states by using the encoder model and the gyroscope model. The error estimates were continuously fedback to the encoder model to correct the wheelchair positions and its heading angles, in order to obtain the filtered position and heading angle.

3.1.2 Odometry model

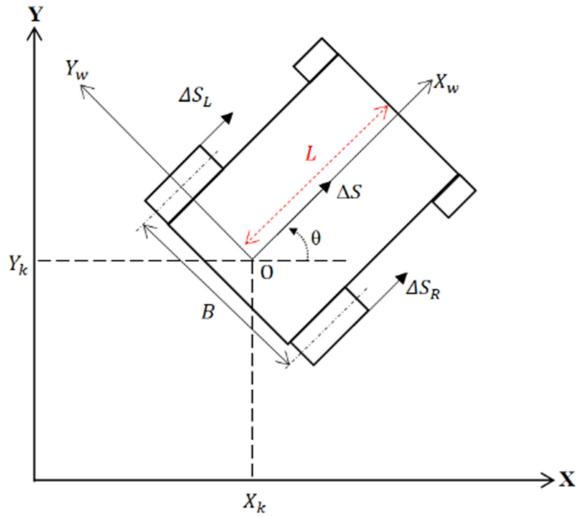

Figure 3.2: A differential drive wheelchair kinematic diagram.

Figure 3.2 shows the kinematic diagram of the differential drive wheelchair with two independently driven wheels. The wheelchair position and the heading angle of the theoretical model were calculated by using the differential drive kinematic Eq. (3.1) to Eq. (3.4) as shown below:

$$X_{k+1} = X_k + \Delta S_k cos(\theta_k) \tag{3.1}$$

$$Y_{k+1} = Y_k + \Delta S_k sin(\theta_k) \tag{3.2}$$

$$\theta_{k+1} = \theta_k + \frac{\Delta S_{R,k} - \Delta S_{L,k}}{\mathrm{B}} \tag{3.3}$$

$$\Delta S_k = \frac{\Delta S_{R,k} + \Delta S_{L,k}}{2} \tag{3.4}$$

where

ΔS_L , ΔS_R : left and right wheels incremental encoder distance, respectively

X_w , Y_w : wheelchair body frame

X_k , Y_k : wheelchair coordinates on navigation frame

X , Y : Navigation frame

θ : Orientation of the wheelchair with respect to navigation frame

B : Wheelbase size

O : Origin point of wheelchair

L : Distance between front of wheelchair to origin point of wheelchair 670mm

The two most dominant systematic errors -- the wheelbase error, ∂B_k and the right and left wheel scale factor errors ($c_{R,k}$, $c_{L,k}$) were taken into consideration in computing the position and the heading angle of the wheelchair with the practical encoder model (Eq. (3.5) to Eq. (3.11)). $\hat{X}_k$, $\hat{Y}_k$ and $\hat{\theta}_k$ are the encoder position and the heading angle of the practical encoder model while $\partial\hat{X}_k$, $\partial\hat{Y}_k$ and $\partial\hat{\theta}_k$ are the encoder position and the heading angle errors.

$$\Delta\hat{S}_k = \frac{\Delta S_{R,k} + c_{R,k}\Delta S_{R,k} + \Delta S_{L,k} + c_{L,k}\Delta S_{L,k}}{2} \tag{3.5}$$

$$\hat{X}_{k+1} = \hat{X}_k + cos\hat{\theta}_k\left(\frac{\Delta S_{R,k} + c_{R,k}\Delta S_{R,k} + \Delta S_{L,k} + c_{L,k}\Delta S_{L,k}}{2}\right) \tag{3.6}$$

$$\hat{Y}_{k+1} = \hat{Y}_k + sin\hat{\theta}_k\left(\frac{\Delta S_{R,k} + c_{R,k}\Delta S_{R,k} + \Delta S_{L,k} + c_{L,j}\Delta S_{L,k}}{2}\right) \tag{3.7}$$

$$\hat{\theta}_{k+1} = \hat{\theta}_k + \frac{\left(\Delta S_{R,k} + c_{R,k}\Delta S_{R,k}\right) - \left(\Delta S_{L,k} + c_{L,k}\Delta S_{L,k}\right)}{\mathrm{B} + \partial B_k} \tag{3.8}$$

$$\hat{X}_k = X_k + \partial X_k \tag{3.9}$$

$$\hat{Y}_k = Y_k + \partial Y_k \tag{3.10}$$

$$\hat{\theta}_k = \theta_k + \partial\theta_k \tag{3.11}$$

The error propagation equations were obtained by subtracting the theoretical position values from the practical position values.

$$\partial X_{k+1} = \partial X_k + cos\theta_k \frac{\Delta S_{R,k}}{2}.c_{R,k} + cos\theta_k \frac{\Delta S_{L,k}}{2}.c_{L,k} - sin\theta_k \frac{\Delta S_{R,k} + \Delta S_{L,k}}{2}.\partial\theta_k \tag{3.12}$$

$$\partial Y_{k+1} = \partial Y_k + sin\theta_k \frac{\Delta S_{R,k}}{2}.c_{R,k} + sin\theta_k \frac{\Delta S_{L,k}}{2}.c_{L,k} + cos\theta_k \frac{\Delta S_{R,k} + \Delta S_{L,k}}{2}.\partial\theta_k \tag{3.13}$$

$$\partial\theta_{k+1} = \partial\theta_k + \frac{\Delta S_{R,k}}{\mathrm{B}} c_{R,k} - \frac{\Delta S_{L,k}}{\mathrm{B}} c_{L,k} + \frac{\Delta S_{L,k} - \Delta S_{R,k}}{\mathrm{B}^2} \partial B_k \tag{3.14}$$

It was assumed that there was no wheel alignment error in the system and the value of $\partial\theta$ was small. Therefore, $\sin(\partial\theta_k) \approx \partial\theta_k$, $\cos(\partial\theta_k) \approx 1, \partial\theta_k c_{R,k} \approx 0$, $\partial\theta_k c_{L,k} \approx 0$ and $\mathrm{B} \gg \partial B_k$.

The wheelbase error and the scale factor error for the left and the right wheel were considered as random constants because these errors had slight variations over time, therefore $c_{R,k+1} = c_{R,k}$, $c_{L,k+1} = c_{L,k}$ and $\partial B_{k+1} = \partial B_k$.

3.1.3 Gyroscope model

Bias drifts and scale factor errors are the two most dominant causes of gyroscope errors. When the gyroscope was at stationary positions, there was always an offset value (gyroscope bias) due to the design imperfection.

The theoretical gyroscope equation is as follow:

$$\Phi_{k+1} = \Phi_k + \Delta\Phi_{k+1} \tag{3.15}$$

The practical gyroscope equation was affected by the gyroscope scale factor error, μ_k and the bias drift, φ_k:

$$\Delta\widehat{\Phi}_k = \Delta\Phi_k + (\mu_k.\Delta\Phi_k) \tag{3.16}$$

$$\begin{aligned}\widehat{\Phi}_{k+1} &= \widehat{\Phi}_k + \Delta\widehat{\Phi}_k \\ &= \widehat{\Phi}_k + \Delta\Phi_k + (\mu_k.\Delta\Phi_k) + \varphi_k\end{aligned} \tag{3.17}$$

where Φ_k and $\widehat{\Phi}_k$ are the theoretical and the practical gyroscope heading angles, respectively. The scale factor error,$\mu_k$and bias drift, $\varphi_k$are considered as random constants. Therefore $\mu_{k+1} = \mu_k$and $\varphi_{k+1} = \varphi_k$.

In this study, the scale factor error of gyroscope was assumed to be zero. The gyroscope bias drift was determined by taking an average of 70 samples of gyroscope reading whenever the wheelchair stops. This gyroscope bias drift was subtracted from the gyroscope readings when it is moved.

The gyroscope error equation was obtained by subtracting the theoretical gyroscope equation from the estimated gyroscope equation:

$$\partial\Phi_{k+1} = \partial\Phi_k + \mu_k.\Delta\Phi_k + \varphi_k \tag{3.18}$$

From Eq. (3.18),

$$\Delta\Phi_k = \frac{\Delta\widehat{\Phi}_k}{(1+\mu_k)} \tag{3.19}$$

Therefore,

$$\partial\Phi_{k+1} = \partial\Phi_k + \mu_k . \frac{\Delta\widehat{\Phi}_k}{(1+\mu_k)} + \varphi_k \tag{3.20}$$

3.1.4 Kalman filter model

The Kalman filter algorithm worked in a two-step process -- prediction and update.

In the prediction stage, the predicted state estimate $\hat{x}_{k|k-1}$ and the predicted covariance estimate, $P_{k|k-1}$ at time k were computed by using the equations below where the control input, u_k= 0 for current work:

$$\hat{x}_{k|k-1} = F_k \hat{x}_{k-1|k-1} + B_k u_k + w_k \tag{3.21}$$

$$P_{k|k-1} = F_k P_{k-1|k-1} F_k^T + Q_k \tag{3.22}$$

When the Kalman filter proceeded to the update stage, innovation, $\widetilde{y}_k$ was computed by taking the difference between the actual and the predicted measurements.

$$\widetilde{y}_k = z_k - H_k \hat{x}_{k|k-1} \tag{3.23}$$

$$K_k = P_{k|k-1} H_k^T (R_k + H_k P_{k|k-1} H_k^T)^{-1} \tag{3.24}$$

Kalman gain matrix, K_k was used to measure the relative confidence of the measurement and prediction. The Kalman gain was small when the measurement noise was high causing the filter to place more weight to prediction instead of measurement.

$$\hat{x}_{k|k} = \hat{x}_{k|k-1} + K_k \tilde{y}_k \tag{3.25}$$

$$P_{k|k} = (I - K_k H_k) P_{k|k-1} \tag{3.26}$$

$$\begin{bmatrix} \partial X_{k+1} \\ \partial Y_{k+1} \\ \partial \theta_{k+1} \\ c_{R,k+1} \\ c_{L,k+1} \\ \partial B_{k+1} \\ \partial \Phi_{k+1} \\ \mu_{k+1} \\ \varphi_{k+1} \end{bmatrix} = \begin{bmatrix} 1 & 0 & -sin\theta_k \frac{\Delta S_{R,k}+\Delta S_{L,k}}{2} & cos\theta_k \frac{\Delta S_{R,k}}{2} & cos\theta_k \frac{\Delta S_{L,k}}{2} & 0 & 0 & 0 & 0 \\ 0 & 1 & cos\theta_k \frac{\Delta S_{R,k}+\Delta S_{L,k}}{2} & sin\theta_k \frac{\Delta S_{R,k}}{2} & sin\theta_k \frac{\Delta S_{L,k}}{2} & 0 & 0 & 0 & 0 \\ 0 & 0 & 1 & \frac{\Delta S_{R,k}}{B} & -\frac{\Delta S_{L,k}}{B} & \frac{\Delta S_{L,k}-\Delta S_{R,k}}{B^2} & 0 & 0 & 0 \\ 0 & 0 & 0 & 1 & 0 & 0 & 0 & 0 & 0 \\ 0 & 0 & 0 & 0 & 1 & 0 & 0 & 0 & 0 \\ 0 & 0 & 0 & 0 & 0 & 1 & 0 & 0 & 0 \\ 0 & 0 & 0 & 0 & 0 & 0 & 1 & \frac{\Delta\widehat{\Phi}_k}{(1+\mu_k)} & 1 \\ 0 & 0 & 0 & 0 & 0 & 0 & 0 & 1 & 0 \\ 0 & 0 & 0 & 0 & 0 & 0 & 0 & 0 & 1 \end{bmatrix} \begin{bmatrix} \partial X_k \\ \partial Y_k \\ \partial \theta_k \\ c_{R,k} \\ c_{L,k} \\ \partial B_k \\ \partial \Phi_k \\ \mu_k \\ \varphi_k \end{bmatrix} + \text{w} \tag{3.27}$$

The updated state estimate,$\hat{x}_{k|k}$ and the updated state covariance, $P_{k|k}$ were computed based on the Kalman gain , K_k.

3.1.5 Implementation of indirect feedback Kalman filter

The state equations of the indirect feedback Kalman filter, $x_{k+1} = Fx_k + w_k$ were shown in Eq. (3.27), where w_k represented the system noise with a covariance, Q. The measurement equation for Kalman filter is given by z_k= Hx_k+ v_k where v_k represents the measurement noise with a covariance, R.

$$z_k = \left(\hat{\theta}_k - \hat{\Phi}_k\right) + v \tag{3.28}$$

Both $\hat{\theta}_k$ and $\hat{\Phi}_k$ are referring to the same angle which is the wheelchair heading angle. Thus, the difference in both angles is also equivalent to the difference of angle error. The difference in the heading angle between the wheel encoder and the gyroscope are taken as the measurement equation given by

$$z_k = (\partial\theta_k - \partial\Phi_k) + v$$

$$z_k = [0 \quad 0 \quad 1 \quad 0 \quad 0 \quad 0 \quad -1 \quad 0 \quad 0] \begin{bmatrix} \partial X_k \\ \partial Y_k \\ \partial\theta_k \\ c_{R,k} \\ c_{L,k} \\ \partial B_k \\ \partial\Phi_k \\ \mu_k \\ \varphi_k \end{bmatrix} + v \tag{3.29}$$

The covariance matrices Q and R were determined and tuned empirically:

Q= diag[$(100mm)^2$,$(100mm)^2$,$(0.001745\ rad)^2$,$(0.00002)^2$, $(0.00002)^2$, $(0.00002)^2$, $(1.7453 \times 10^{-5} rad)^2$, $(0.0001)^2$, $(0.0003)^2$]

R = $(3.4907 \times 10^{-4} rad)^2$

3.2 Experiment setup and procedures

3.2.1 Wheelchair and sensors specifications

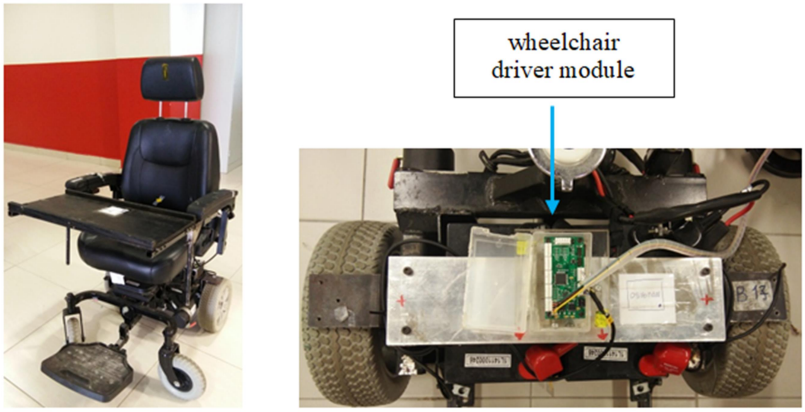

Figure 3.3: Photographs showing the wheelchair used in the current study (left) and the driver module on the wheelchair (right).

The wheelchair used in the current study was a commercial motorized wheelchair (Figure 3.3). The joystick controller was bypassed by using the wheelchair driver module which consisted of a 16–bit microcontroller. Wheel encoders were mounted to the two driving wheels via a pulley system to calculate the distance travelled by the wheelchair. A gyroscope was mounted at the centre of the two driving wheels. The values of the important parameters of the wheelchair and the gyroscope are listed in Table 3.1:

Table 3.1: Wheelchair and gyroscope parameters.

Parameters	Values
Wheel diameter, D	257.8 mm
Wheelbase, B	520 mm
Encoder pulse per revolution	500
Gyroscope full scale range	±250 º/s
Gyroscope sensitivity scale factor	131 LSB / (º /s)
Gyroscope scale factor error, μ_k	0

3.2.2 Measurement of errors in wheelchair navigation system by using odometry

Measurement of systematic errors was performed based on the UMBMark bidirectional square path test (Borenstein and Feng, 1996; Guran et al., 2015; Jung and Chung, 2011; Jung and Chung, 2012; Censi et al., 2013; Luiz et al., 2017; Maddahi et al., 2013). In total 40 runs of square path (4200mmx 4200mm) were performed, with 20 runs in CCW and 20 runs in CW directions using the odometry method. The details of the experimental procedure are explained below:

1. Wheelchair was placed at a designated starting point where its absolute position and odometry position were both (0,0).
2. The wheelchair was programmed to travel in a 4200mm x 4200mm square path in CCW or CW direction by :
    a. Stopping after each 4200 mm straight motion
    b. Making a total of four 90° on the spot turning
    c. Running the wheelchair slowly to avoid wheel slippage

3. After completing the run in a square path by returning to the start position, the absolute X-Y position of the wheelchair on the floor was measured.
4. The absolute position of the wheelchair was compared with the calculated odometry position.

In this experiment, the linear and angular velocities of the wheelchair were tuned to constant values of 200mm s^{-1} and 0.35 rad s^{-1} respectively to minimize wheel slippage. Measurements for different linear and angular speeds were not performed as they involved calculations of non-systematic errors such as wheel slippage and friction with the floor, which were not taken into consideration in the current study. The position and orientation of the wheelchair were updated every 50ms. The return position errors were computed based on the following equations:

$$\varepsilon_x = x_{abs} - x_{calc} \tag{3.30}$$

$$\varepsilon_y = y_{abs} - y_{calc} \tag{3.31}$$

where

$\varepsilon_x, \varepsilon_y$: position errors due to odometry

x_{abs}, y_{abs} : wheelchair absolute positions measured from the floor

x_{calc}, y_{calc} : positions calculated from odometry

The return position errors were used to compute the centre of gravity for both CCW and CW directions as follow:

$$x_{c.g,CCW/CW} = \frac{1}{n}\sum_{i=1}^{n} \varepsilon x_{i,CCW/CW} \tag{3.32}$$

$$y_{c.g,CCW/CW} = \frac{1}{n}\sum_{i=1}^{n} \varepsilon y_{i,CCW/CW} \tag{3.33}$$

where n is the number of runs in each direction.

3.2.3 Calculation of wheelbase error(∂B) and scale factor error(c_L, c_R)

By using the result from Section 3.2.2, orientation errors α (due to Type A error) and β (due to Type B error) were calculated. Type A error was caused by uncertainties of wheelbase and Type B error was caused by unequal wheel diameters. Type A error was defined as the orientation error that increased (or reduced) the total angle of rotation of the wheelchair when it was run in both CCW and CW directions in the square path. Type B error was defined as the orientation error that increased (or reduced) the total angle of rotation of the wheelchair when it was run in one direction but reduced (or increased) the total angle of rotation of the wheelchair when it was run in another direction. Both types of errors occurred together in actual runs. In CCW direction, errors added up to each other leading to an increase in the overall error. On the other hand, the errors compensated for each other in CW direction (Appendix A).

These values were used to calculate the wheelchair scale factor error (c_L, c_R) and wheelbase error (∂B). The detailed derivation of the formula is shown in Eq. (3.34) to Eq. (3.61) by making the following assumptions (Borenstein and Feng, 1996; Ruan et al., 2012; Jung and Chung, 2011; Luiz et al., 2017):

1. The main sources of odometry errors were wheelbase error and errors caused by unequal wheel diameter.
2. Turning motion error was caused only by the wheelbase error, E_b.
3. Straight line motion error was caused only by unequal wheel diameter, E_d.
4. Type A error was caused only by E_b
5. Type B error was caused only by E_d
6. Due to the 4th assumption shown above, Type A errors could be eliminated almost completely by eliminating E_b
7. Due to the 5th assumption shown above, Type A errors could be eliminated almost completely by eliminating E_d

The analysis of Type A and Type B errors was carried out by assuming the wheelchair initial position (x_o, y_o) was (0,0). Small angle approximation was made by assuming $L\sin\gamma \approx L\gamma$ and $L\cos\gamma \approx L$, where L is the length of the sides of the square path.

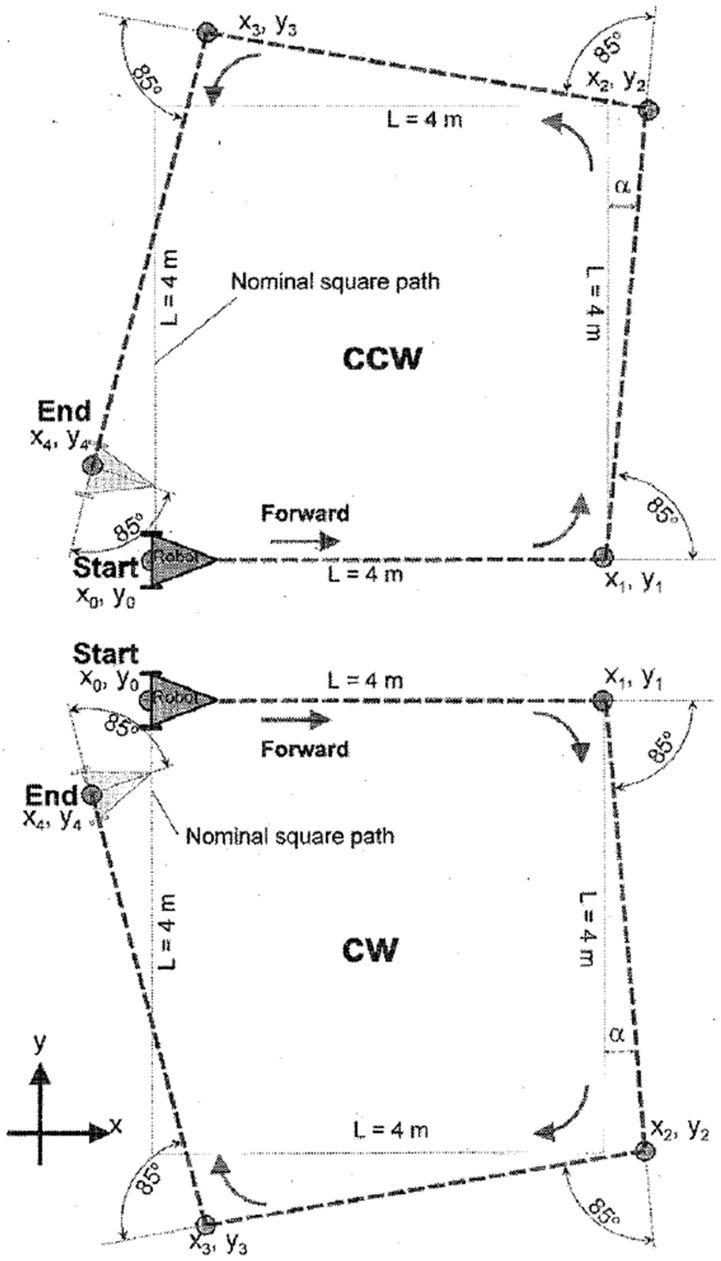

Figure 3.4: Type A errors in CCW and CW directions.

Type A error would lead to rotation greater or lesser than the nominal 90◦ turn at the square path corners as shown in Figure 3.4 .Therefore, α(rad) is the amount of orientation error in each nominal 90◦ turn.

Type A errors in CCW direction:

$$x_1 = x_o + L \tag{3.34a}$$

$$y_1 = y_o \tag{3.34b}$$

$$x_2 = x_1 + \ Lsin\alpha \approx L + L\alpha \tag{3.35a}$$

$$y_2 = y_1 + \ Lcos\alpha \approx L \tag{3.35b}$$

$$x_3 = x_2 - Lcos2\alpha \approx L\alpha \tag{3.36a}$$

$$y_3 = y_2 + \ Lsin2\alpha \approx L + 2L\alpha \tag{3.36b}$$

$$x_4 = x_3 - Lsin3\alpha \approx -2L\alpha \tag{3.37a}$$

$$y_4 = y_3 - \ Lcos3\alpha \approx 2L\alpha \tag{3.37b}$$

Type A errors in CW direction:

$$x_1 = x_o + L \tag{3.38a}$$

$$y_1 = y_o \tag{3.38b}$$

$$x_2 = x_1 + \ Lsin\alpha \approx L + L\alpha \tag{3.39a}$$

$$y_2 = y_1 - \ Lcos\alpha \approx -L \tag{3.39b}$$

$$x_3 = x_2 - Lcos2\alpha \approx L\alpha \tag{3.40a}$$

$$y_3 = y_2 - \ Lsin2\alpha \approx -L - 2L\alpha \tag{3.40b}$$

$$x_4 = x_3 - Lsin3\alpha \approx -2L\alpha \tag{3.41a}$$

$$y_4 = y_3 + Lcos3\alpha \approx -2L\alpha \tag{3.41b}$$

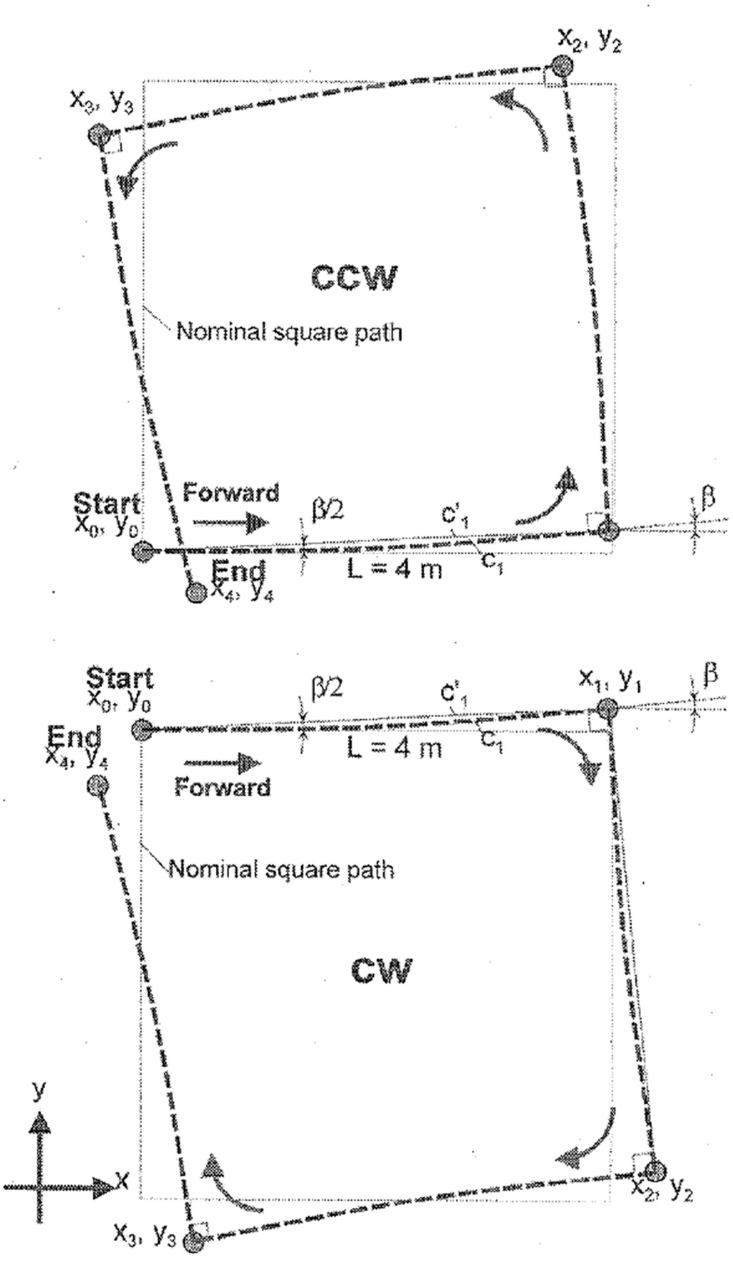

Figure 3.5: Type B errors in CCW and CW directions. (Adapted from Borenstein and Feng, 1996)

Type B error caused the wheelchair to travel in a slightly curvy trajectory instead of moving straight as shown in Figure 3.5. Therefore, the wheelchair would gain an orientation error known as β (rad) at the end of each straight trajectory in the square path. The auxiliary line c_1' connected the points

at the corner of actual path was parallel to the arc $c_1$midpoint resulting in a slope of $\beta/2$. Thus, the equations for Type B error were computed based on β. Type B errors in CCW direction:

$$x_1 = x_o + Lcos(\beta/2) \approx L \quad (3.42a)$$

$$y_1 = y_o + Lsin(\beta/2) \approx L\beta/2 \quad (3.42b)$$

$$x_2 = x_1 - Lsin(3\beta/2) \approx L - 3L\beta/2 \quad (3.43a)$$

$$y_2 = y_1 + Lcos(3\beta/2) \approx L\beta/2 + L \quad (3.43b)$$

$$x_3 = x_2 - Lcos(5\beta/2) \approx -3L\beta/2 \quad (3.44a)$$

$$y_3 = y_2 - Lsin(5\beta/2) \approx -2L\beta + L \quad (3.44b)$$

$$x_4 = x_3 + Lsin(7\beta/2) \approx 2L\beta \quad (3.45a)$$

$$y_4 = y_3 - Lcos(7\beta/2) \approx -2L\beta \quad (3.45b)$$

Type B errors in CW direction:

$$x_1 = x_o + Lcos(\beta/2) \approx L \quad (3.46a)$$

$$y_1 = y_o + Lsin(\beta/2) \approx L\beta/2 \quad (3.46b)$$

$$x_2 = x_1 + Lsin(3\beta/2) \approx L + 3L\beta/2 \quad (3.47a)$$

$$y_2 = y_1 - Lcos(3\beta/2) \approx L\beta/2 - L \quad (3.47b)$$

$$x_3 = x_2 - Lcos(5\beta/2) \approx 3L\beta/2 \quad (3.48a)$$

$$y_3 = y_2 - Lsin(5\beta/2) \approx -L(2\beta + 1) \quad (3.48b)$$

$$x_4 = x_3 - Lsin(7\beta/2) \approx -2L\beta \quad (3.49a)$$

$$y_4 = y_3 + Lcos(7\beta/2) \approx -2L\beta \quad (3.49b)$$

The orientation error α and β were obtained by superimposing Type A error and Type B error equations in x –direction.

$$x_{CW}: -2L\alpha - 2L\beta = -2L(\alpha + \beta) = x_{c.g.,CW} \tag{3.50}$$

$$x_{CCW}: -2L\alpha + 2L\beta = -2L(\alpha - \beta) = x_{c.g.,CCW} \tag{3.51}$$

Subtracting (3.51) from (3.50)

$$-4L\beta = x_{c.g.,CW} - x_{c.g.,CCW} \tag{3.52}$$

or,

$$\beta = \frac{x_{c.g.,CW} - x_{c.g.,CCW}}{-4L}\frac{(180°)}{\pi} \tag{3.53a}$$

β could be calculated from the terms in y-direction as follow :

$$\beta = \frac{y_{c.g.,CW} + y_{c.g.,CCW}}{-4L}\frac{(180°)}{\pi} \tag{3.53b}$$

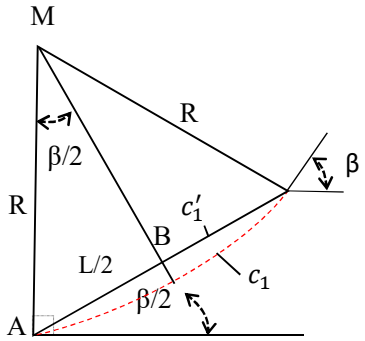

Figure 3.6: Radius of curvature geometric relations. (Adapted from Borenstein and Feng, 1996)

From triangle ABM in Figure 3.6, the curved path radius of curvature, R in Figure 3.6 was computed by using simple geometric calculation:

$$R = \frac{L/2}{\sin(\beta/2)} \tag{3.54}$$

The radius of curvature, R obtained was used to compute the right and left wheel diameter ratio, E_d:

$$E_d = \frac{D_R}{D_L} = \frac{R + b/2}{R - b/2} \tag{3.55}$$

α value could be obtained by adding Eq. (3.50) and Eq. (3.51) in the x-direction or by comparing the terms in the y-direction as shown below :

$$\alpha = \frac{x_{c.g.,CW} + x_{c.g.,CCW}}{-4L} \frac{(180°)}{\pi} \tag{3.56}$$

or

$$\alpha = \frac{y_{c.g.,CW} - y_{c.g.,CCW}}{-4L} \frac{(180°)}{\pi} \tag{3.57}$$

The α value was used to calculate the wheelbase error, E_b where $B_{nominal}$ and B_{actual} represent the nominal and the actual wheelbase, respectively. The equation for obtaining wheelbase error was as follow:

$$E_b = \frac{B_{actual}}{B_{nominal}} = \frac{90°}{90° - \alpha} \tag{3.58}$$

The correction factors: c_L,c_R and ∂B were calculated by using the equations below :

$$c_L = \frac{2}{E_d + 1} \tag{3.59}$$

$$c_R = \frac{2}{(1/E_d) + 1} \tag{3.60}$$

$$\partial B = B_{actual} - B_{nominal} \tag{3.61}$$

3.2.4 Comparison of square path experiment performance by using odometry and that by sensor fusion of encoder and gyroscope using indirect feedback Kalman filter

A total of 40 runs of square path in CCW and CW directions were conducted by using the indirect feedback Kalman filter method. The experimental procedure was the same as section 3.2.2. The measured distance error in Eq. (3.62) was used for comparison between experiments that were performed by using odometry and sensor fusion of encoder and gyroscope using indirect feedback Kalman filter. Final orientation error was not taken into account because the systematic errors had been translated into position errors due to the fixed-length sides of the square path (Borenstein and Feng, 1996).

$$Measured\ distance\ error = \sqrt{\varepsilon_x^2 + \varepsilon_y^2} \tag{3.62}$$

The dispersion of each category of data was measured by using the standard distance. It was depicted graphically by drawing a circle around the mean centre of distribution where the radius of circle was equivalent to the standard distance (Burt et al., 2009). The formula was defined as:

$$SD = \sqrt{\frac{\sum_{i=1}^{n}(X_i - \bar{X})^2}{n} + \frac{\sum_{i=1}^{n}(Y_i - \bar{Y})^2}{n}} \tag{3.63}$$

where

n is the total set of coordinates

i = 1,2,3….n

(X_i,Y_i) are the coordinates

The error percentage of the distance error was computed using the equation below:

$$Error\ \% = \frac{Distance\ error}{Total\ distance\ travelled} \times 100\% \tag{3.64}$$

In order to test the effectiveness of the indirect feedback Kalman filter in a larger square path, experiments were repeated in a 9000mm x 9000mm square path. A total of 20 runs were performed, 10 runs in CCW and another 10 runs in CW directions.

CHAPTER 4

RESULTS AND DISCUSSION

4.1 Odometry errors in the wheelchair navigation system

Table 4.1: Return position errors (εX,εY and measured distance) of the wheelchair using odometry.

# of trial	CCW			CW		
	εX (mm)	**εY (mm)**	**Measured distance error (mm)**	**εX (mm)**	**εY (mm)**	**Measured distance error (mm)**
1	-429	494	654.28	46	28	53.85
2	-409	511	654.52	42	33.5	53.72
3	-371	495	618.60	28	32	42.52
4	-396	478	620.73	34	20	39.45
5	-395	467	611.65	24	9	25.63
6	-400	514	651.30	50	33	59.91
7	-379	510	635.41	43	8	43.74
8	-378	458	593.84	60	12	61.19
9	-384	473	609.25	41	10	42.20
10	-371	449	582.44	27	18	32.45
11	-378	459	594.61	51	42	66.07
12	-344	397	525.30	35	20	40.31
13	-350	464	581.20	28	7	28.86
14	-354	461	581.24	32	-2	32.06
15	-383	445	587.12	47	-2	47.04
16	-361	473	595.02	26	-7	26.93
17	-380	486	616.92	18	17	24.76
18	-356	472	591.20	-10	-17	19.72
19	-363	461	586.76	0	-36	36.00
20	-469	474	666.81	1	-18	18.03
Mean	**-382.50**	**472.05**	**607.91**	**31.15**	**10.38**	**39.72**
Standard Deviation	**28.47**	**26.04**	**32.71**	**17.74**	**19.30**	**13.68**

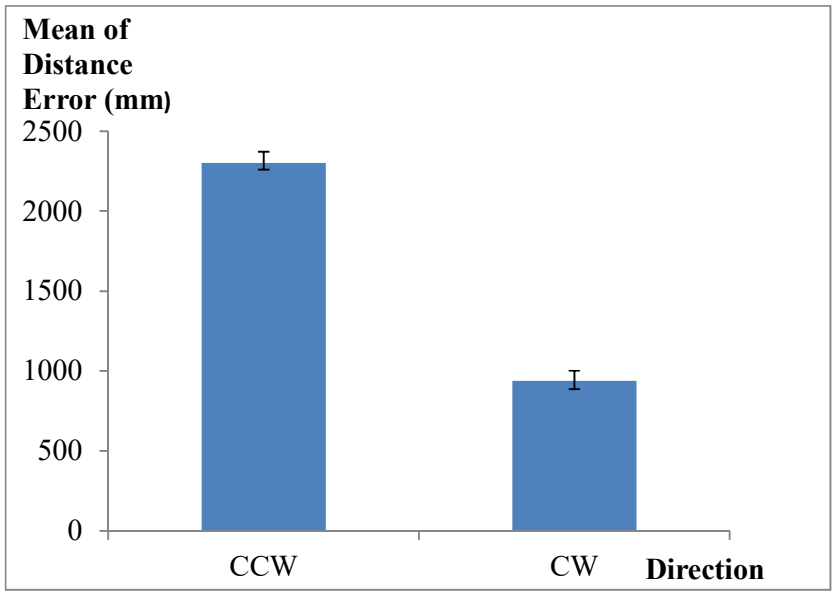

Figure 4.1: Mean of distance error of the wheelchair using odometry. Data are mean ± SD.

Table 4.1 shows the return position errors of the wheelchair using odometry. It was observed that the measured distance errors for CCW and CW directions lie in the range of 525mm to 667mm and 18mm to 66mm, respectively.

The CCW mean of distance error was about five times greater than the CW mean of distance error (Figure 4.1). This was due to the two dominant systematic errors in the wheelchair which cancelled off each other in the CW direction while added up to each other in the CCW direction (Figure 4.2). It was observed that Figure 4.2 was similar to Figure A.1 in Appendix A where the trajectory of the robot or wheelchair was closer to the reference path in CW direction and further from the reference path in CCW direction.

(a)

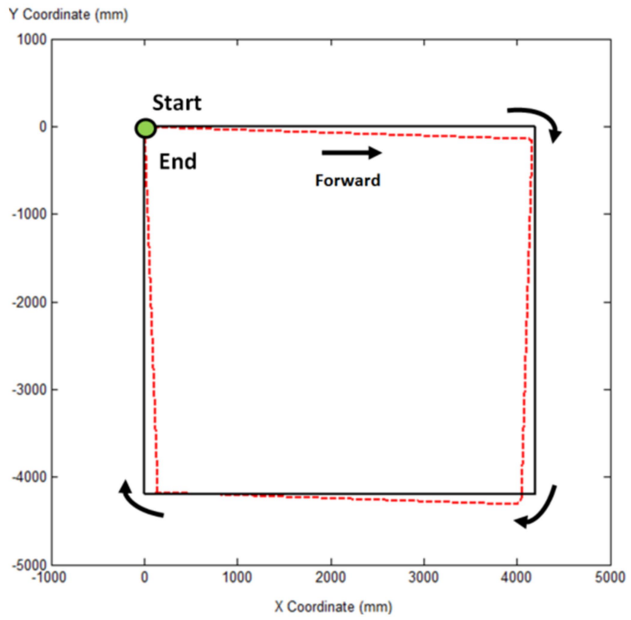

(b)

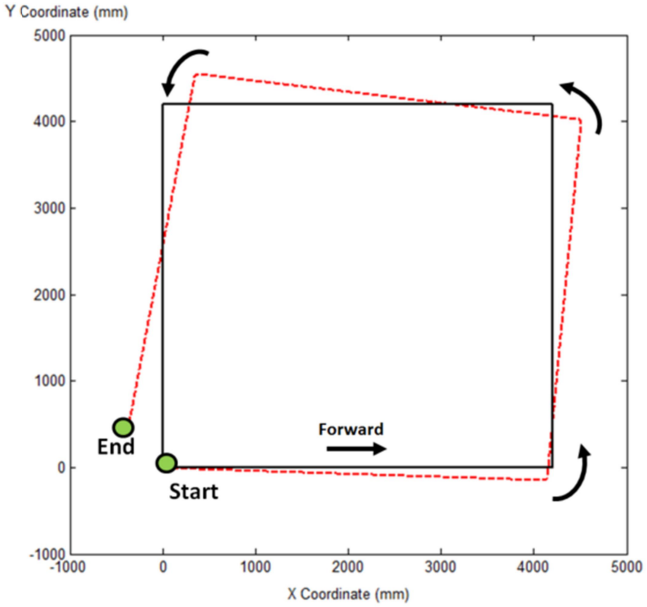

Figure 4.2: Trajectory of wheelchair in a square path experiment obtained using odometry. The red dash line represents the wheelchair trajectory and the black line represents the reference square path. The figure showed the effect of the two dominant systematic errors of wheelchair in (a) CW and (b) CCW directions.

Table 4.2: The orientation errors of the wheelchair.

Odometry (α, degree)		Odometry (β, degree)	
x-direction	y-direction	x-direction	y-direction
1.1982	1.5745	-1.4107	-1.6453

By using the return position errors from Table 4.1, the orientation errors α and β were calculated (Table 4.2). α and β are important parameters needed for the calculation of the wheelchair correction factors. Theoretically, the values of α and β should be the same in both the x and y directions (Borenstein and Feng, 1996). However, slight differences were observed, possibly due to the non-systematic errors that were not taken into consideration in this study.

The wheelbase error ratio, E_b and the unequal wheel diameter ratio, E_d were calculated based on: 1) α_x and β_x and 2) α_y and β_y. To minimize the effect of non-systematic errors, therefore, the wheelchair correction factors were computed using the average of $E_{b,x}$ and $E_{b,y}$ as well as $E_{d,x}$ and $E_{d,y}$, respectively. These correction factors were then used as the initial values in the state space model of the indirect feedback Kalman filter equations.

Table 4.3: Wheelbase and wheel scale factor errors.

∂B	8.1379mm
c_R	-0.001650
c_L	0.001650

Based on the data in Table 4.3, the actual wheelbase of the wheelchair was approximated to be 528.1379 mm instead of the nominal value of 520mm.

The right wheel diameter was found to be relatively smaller than that of the left wheel (0.33%). The computed data was used to correct the wheelbase and wheel diameters.

4.2 Comparison of the wheelchair navigation performance by using odometry and that by sensor fusion of encoder and gyroscope using indirect feedback Kalman filter

Table 4.4: Return position errors (εX,εY and measured distance errors) of wheelchair using sensor fusion of encoder and gyroscope along a 4200mm x 4200mm square in both CCW and CW directions.

# of trial	CCW			CW		
	εX (mm)	**εY (mm)**	**Measured distance error (mm)**	**εX (mm)**	**εY (mm)**	**Measured distance error (mm)**
1	50	13	51.66	47	30	55.76
2	66	37	75.66	46	21	50.57
3	-1	73	73.01	57	37	67.96
4	48	61	77.62	27	15	30.89
5	23	54	58.69	30	17	34.48
6	48	40	62.48	67	43	79.61
7	51	87	100.85	47	20	51.08
8	12	63	64.13	40	16	43.08
9	10	61	61.81	14	12	18.44
10	-15	89	90.26	33	-13	35.47
11	26	64	69.08	23	-46	51.43
12	21	71	74.04	46	20	50.16
13	-7	68	68.36	47	41	62.37
14	13	66	67.27	44	9	44.91
15	21	58	61.68	10	0	10.00
16	-47	114	123.31	22	18	28.43
17	5	92	92.14	28	11	30.08
18	1	89	89.01	17	2	17.12
19	13	90	90.93	84	5	84.15
20	-22	100	102.39	49	36	60.80
Mean	**15.80**	**69.50**	**77.72**	**38.90**	**14.70**	**45.34**
Standard Deviation	**27.14**	**23.07**	**17.56**	**17.92**	**19.71**	**19.58**

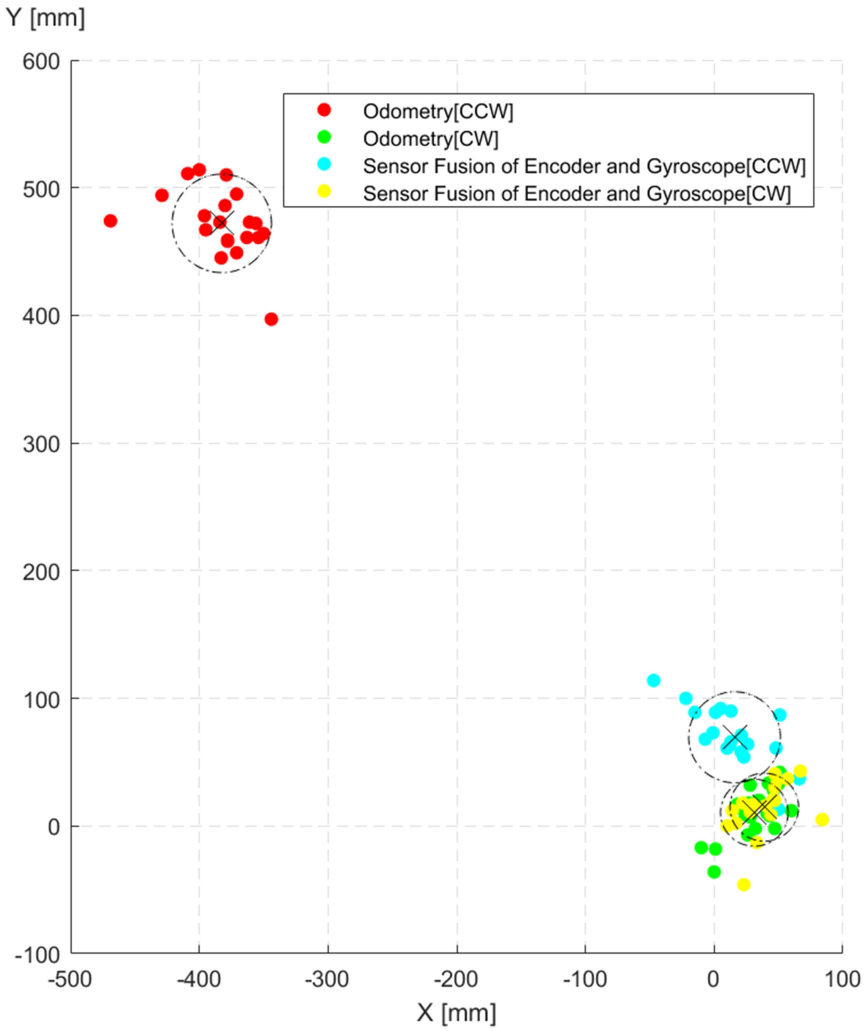

Figure 4.3: Return position errors (εX and εY) of wheelchair using odometry and that by sensor fusion of encoder and gyroscope. The radius of the circles represents the standard distance.

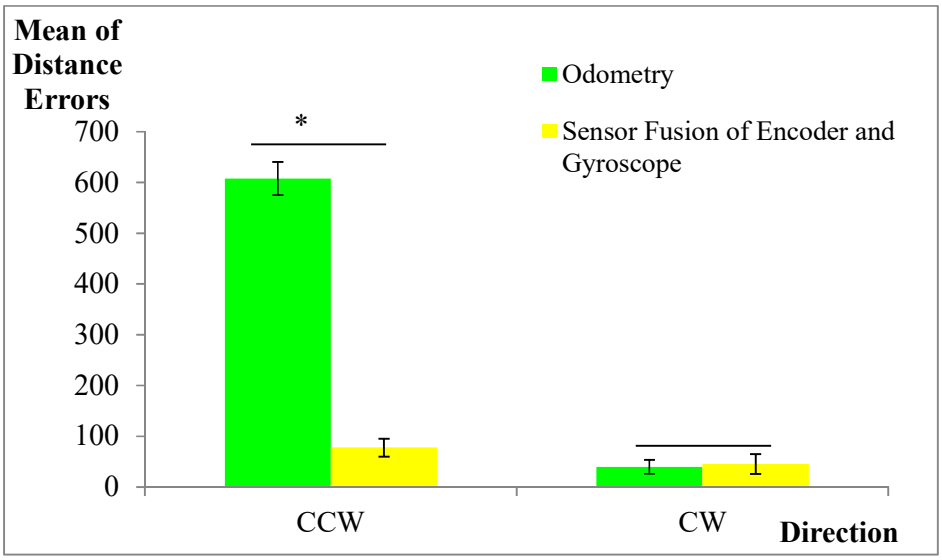

Figure 4.4: Comparison of the mean of distance error of wheelchair using odometry and that by sensor fusion of encoder and gyroscope. Data are means ± SD. * indicates significant difference at $p<0.05$.

Table 4.4 shows the return position errors for the wheelchair using sensor fusion of encoder and gyroscope. It was observed that the measured distance errors for CCW and CW directions lie in the range of 51mm to 123mm and 10mm to 84mm, respectively.

From Figure 4.3, it was observed that the centre of gravity of wheelchair using odometry for CCW direction was further from the (0,0) position. For CW direction, the centre of gravity was closer to the (0,0) position. On the other hand, the centre of gravity of wheelchair using sensor fusion of encoder and gyroscope for both CCW and CW directions were closer to the (0,0) position.

The comparison of the wheelchair's mean of distance error was shown in Figure 4.4. In the CCW direction, the mean of distance error of the wheelchair using sensor fusion of encoder and gyroscope was found to have significantly improved (Figure 4.4; $t(38) = 62.241$, $p < .05$,$B = \infty$). On the other hand, no significant difference was observed in the CW direction (Figure 4.4; $t(38) = -1.025$, $p = 0.312$, $B = 0.0545$).

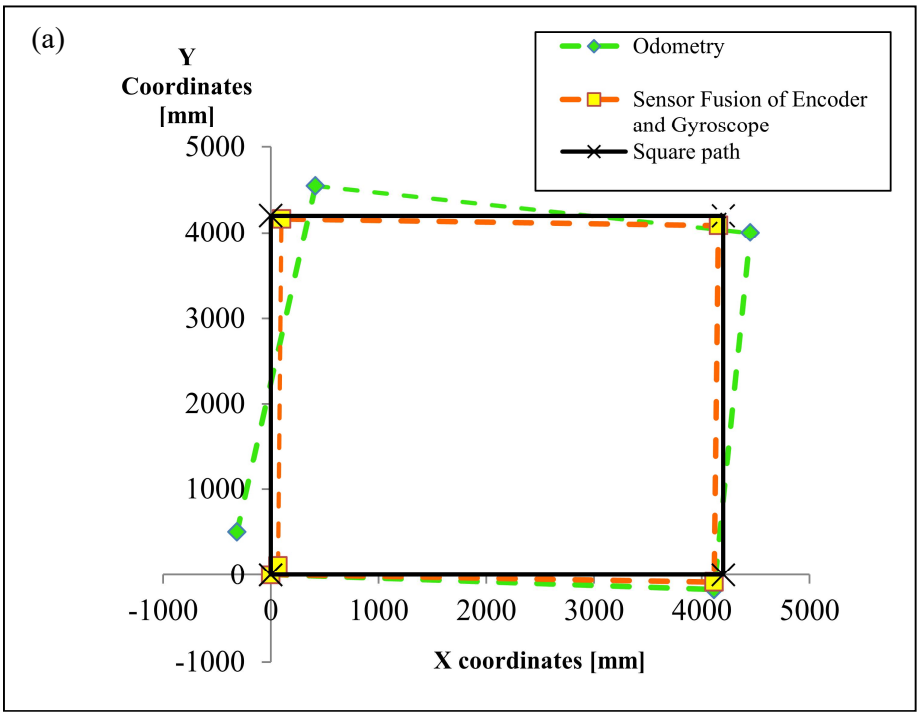

Figure 4.5: Trajectories of the wheelchair in a 4200mm x4200mm square path in (a) CCW and (b) CW directions.

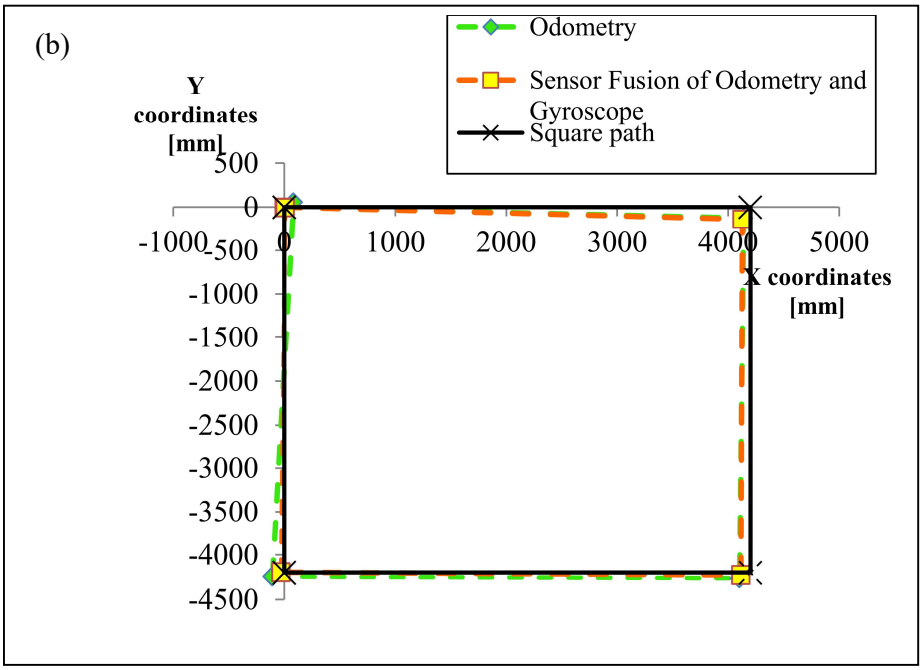

(Figure 4.5, continued)

The trajectories of the wheelchair in the 4200mm x4200mm square were obtained by plotting the absolute position of the wheelchair when it stopped at the four corners of the square. It was notable that the wheelchair using sensor fusion of encoder and gyroscope navigated closer to the square path in the CCW direction (Figure 4.5a). Not much improvement was seen with the sensor fusion of encoder and gyroscope in the CW direction (Figure 4.5b), as expected since the original trajectory was already close to the square path.

The standard distance of the four sets of data (Figure 4.3) were found to be less than 40mm (or 0.24% of the total distance travelled), indicating that the navigation system was precise and repeatable. To further demonstrate the effectiveness of the developed system, the study was repeated on a 9000mm x9000mm square path.

4.3 Comparison of the wheelchair navigation performance by using odometry and that by sensor fusion of encoder and gyroscope using indirect feedback Kalman filter in 9000mm x 9000mm square path

Table 4.5: Return position errors (εX,εY and measured distance errors) of wheelchair using odometry along a 9000mm x 9000mm square in both CCW and CW directions.

# of trial	CCW			CW		
	εX (mm)	εY (mm)	Measured distance error (mm)	εX (mm)	εY (mm)	Measured distance error (mm)
1	-1435	1887	2370.65	747	651	990.86
2	-1412	1898	2365.62	750	721	1040.36
3	-1449	1817	2324.02	583	577	820.25
4	-1418	1822	2308.77	636	579	860.08
5	-1363	1771	2234.77	656	617	900.57
6	-1369	1775	2241.60	705	627	943.48
7	-1390	1784	2261.58	679	642	934.45
8	-1387	1797	2270.02	690	723	999.41
9	-1379	1717	2202.21	730	647	975.45
10	-1480	1941	2440.88	653	625	903.90
Mean	**-1408.20**	**1820.90**	**2302.01**	**682.90**	**640.90**	**936.88**
Standard Deviation	**35.86**	**64.87**	**70.26**	**50.18**	**47.15**	**64.01**

Table 4.6: Return position errors (εX,εY and measured distance errors) of wheelchair using sensor fusion of encoder and gyroscope along a 9000mm x 9000mm square in both CCW and CW direction.

# of trial	CCW			CW		
	εX (mm)	εY (mm)	Measured distance error (mm)	εX (mm)	εY (mm)	Measured distance error (mm)
1	-68	376	382.10	228	110	253.15
2	-37	335	337.04	142	111	180.24
3	12	278	278.26	199	140	243.31
4	-69	284	292.26	116	112	161.25
5	-105	351	366.37	247	122	275.49
6	-26	333	334.01	108	107	152.03
7	-67	324	330.85	261	148	300.04
8	36	279	281.31	133	77	153.68
9	20	240	240.83	183	52	190.24
10	38	270	272.66	163	139	214.22
Mean	**-26.60**	**307.00**	**311.57**	**178.00**	**111.80**	**212.36**
Standard Deviation	**48.12**	**40.57**	**42.92**	**51.87**	**27.86**	**50.51**

It was observed from Table 4.5 that the measured distance errors for CCW and CW directions of wheelchair using odometry lie in the range of 2202mm to 2440mm and 820mm to 1040mm, respectively.

From Table 4.6, it was observed that the measured distance errors for CCW and CW directions of wheelchair using sensor fusion of encoder and gyroscope lie in the range of 240mm to 382mm and 152mm to 300mm, respectively.

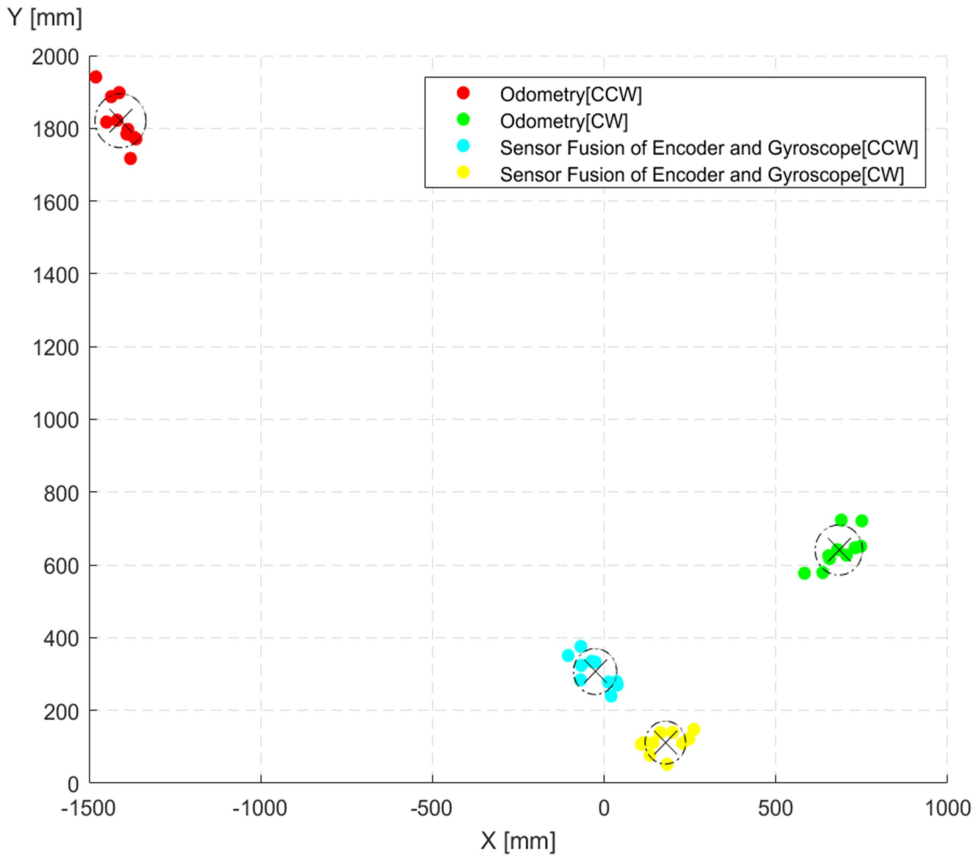

Figure 4.6: Return position errors (εX and εY) of wheelchair along a 9000mm x 9000mm square in both CCW and CW directions. The radius of circle represents the standard distance.

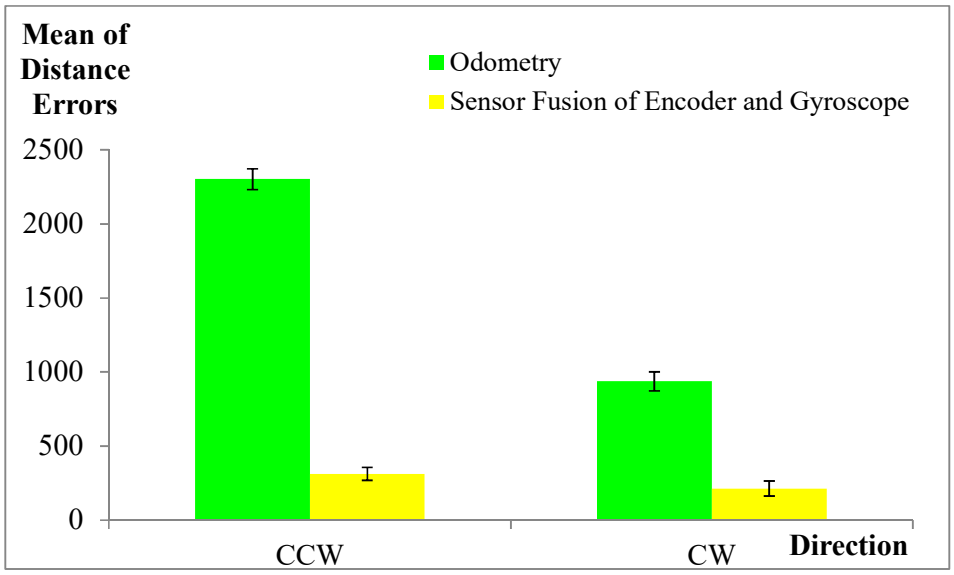

Figure 4.7: Comparison of the mean of distance error of the wheelchair using odometry and sensor fusion of encoder and gyroscope along a 9000mm x9000mm square path. Data were means ± SD.

From Figure 4.6, it was observed that the centre of gravity of wheelchair using odometry for CCW and CW direction were located further from the (0,0) position. The centre of gravity of wheelchair using sensor fusion of encoder and gyroscope for both CCW and CW directions were closer to the (0,0) position.

The comparison of the wheelchair's mean of distance error in a 9000mm x9000mm square path was shown in Figure 4.7. The mean of distance error of the wheelchair had shown an accuracy improvement of 7.4 folds and 4.4 folds in CCW and CW directions, respectively. The consistency of the 9000mm x9000mm square path data were observed from the standard distance of the four sets of data (Figure 4.6), which were less than 80mm (or 0.22% of total distance travelled).

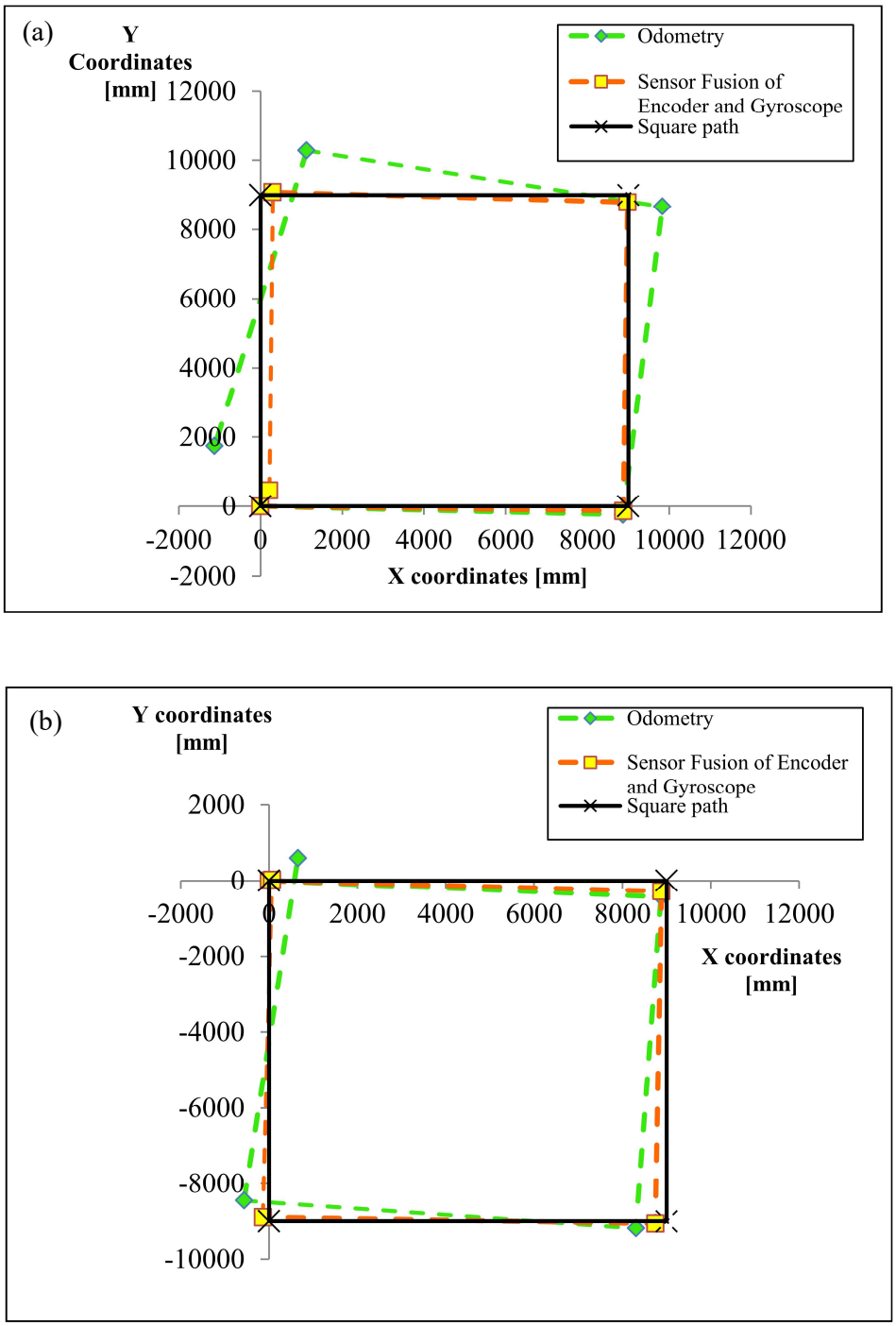

Figure 4.8: Trajectories of the wheelchair in a 9000mm x 9000mm square path in (a) CCW and (b) CW directions.

The method of plotting the trajectories in Figure 4.8 was the same as 4200mm x4200mm square path. For both CCW and CW directions, the

trajectory of wheelchair using odometry were further from the square path whereas the trajectory of wheelchair using sensor fusion of encoder and gyroscope were closer to the square path (Figure 4.8a and Figure 4.8b).

4.4 Discussion

Navigation errors of the wheelchair were minimized by using the difference of the measured orientation angle between the encoder and the gyroscope, indicating that the errors of both sensors were mutually compensated (Park et al., 1996). The gyroscope was chosen in the current work as it was not affected by systematic errors that are caused by wheelchair design imperfection. However, since only the two dominant errors of the wheelchair were considered in this study, integration with the gyroscope only managed to reduce the navigation errors but not eliminating them. The navigation accuracy could be further improved by taking into account other sources of errors such as wheel slippage and irregularities of the floor surface in the wheelchair position and heading angle calculation.

The results obtained from the current study were in agreement with the previous work, which demonstrated that navigation by using odometry integrated with IMU sensors provided estimation of robot position closer to the actual position compared to the odometry system alone. Zhou and Huang (2011) compared the navigation of a mobile robot travelling in a 2.5m x2.0m square path using the odometry system alone and odometry system integrated

with gyroscope and showed that navigation accuracy had improved by 2.9 folds in the latter case. In a separate work, Cho et al. (2011) demonstrated the navigation of a mobile robot in a circular path with a diameter of 9700mm. When the mobile robot navigated using odometry, gyroscope and accelerometer output, it had shown that the navigation accuracy had improved by 2.5 to 4.5 folds compared to odometry alone. Similarly, in the current study, the maximum accuracy improvement was 7.8 folds by using odometry system integrated with gyroscope compared to odometry alone. However, because all the studies were performed using different robots, the improvement in navigation accuracy cannot be directly compared.

CHAPTER 5

CONCLUSION

5.1 Conclusion

The results of the study showed that fusion of encoders and gyroscope using indirect feedback Kalman filter significantly improved the accuracy of the localization of the wheelchair compared to using odometry. The maximum accuracy of improvement in 4200mm x4200mm and 9000mm x 9000mm square paths were 7.8 folds and 7.4 folds, respectively.

The key contributions of this project include:

- Reduction of wheelchair navigation errors where users could reach desired destination within the thumb tip reach (measurement from your shoulder to your thumb tip).

- Enhancement of wheelchair portability by eliminating the need of an onboard computer as the algorithm was incorporated into the wheelchair driver module.

5.2 Recommendations for future work

The current study is limited to wheelchair navigation in an indoor environment where the surface is flat. For future work, three –axis gyroscope, accelerometer, compass and GPS may be integrated in the system to enable wheelchair navigation in an outdoor environment with uneven surface condition and slopes.

REFERENCES

Abbas, T., Arif, M. and Ahmed, W., 2006. Measurement and Correction of Systematic Odometry Errors Caused by Kinematics. 2006 pp. 2073–2078.

Anjum, M.L., Park, J., Hwang, W., Kwon, H. i., Kim, J. h., Lee, C., Kim, K. s., Cho, D. i. "Dan.", 2010. Sensor data fusion using Unscented Kalman Filter for accurate localization of mobile robots. *ICCAS 2010*. 2010 pp. 947–952.

Baatar, G., Eichhorn, M. and Ament, C., 2014. Precise indoor localization of multiple mobile robots with adaptive sensor fusion using odometry and vision data. *IFAC Proceedings Volumes (IFAC-PapersOnline)*. 2014 IFAC, pp. 7182–7189.

Borenstein, J. and Feng, L., 1996. Measurement and Correction of Systematic Odometry Errors in Mobile Robots. *IEEE Transactions on Robotics and Automation*, 12(6), pp.845–857.

Borsje, P., Chan, T.F., Wong, Y.K. and Ho, S.L., 2005. A Comparative Study of Kalman Filtering for Sensorless Control of a Permanent-Magnet Synchronous Motor Drive. *Electric Machines and Drives, 2005 IEEE International Conference on*, pp.815–822.

Burt, J.E., Barber, G.M. and Rigby, D.L., 2009. *Elementary Statistics for Geographers*, The Guilford Press, New York.

Cavanini, L., Cimini, G., Ferracuti, F., Freddi, A., Ippoliti, G., Monteriu, A., Verdini, F., 2017. A QR-code localization system for mobile robots: Application to smart wheelchairs. *2017 European Conference on Mobile Robots (ECMR)*. 2017 pp. 1–6.

Censi, A., Franchi, A., Marchionni, L. and Oriolo, G., 2013. Simultaneous calibration of odometry and sensor parameters for mobile Robots. *IEEE Transactions on Robotics*, 29(2), pp.475–492.

Chang, L., Zha, F. and Qin, F., 2017. Indirect Kalman Filtering Based Attitude Estimation for Low-Cost Attitude and Heading Reference Systems. *IEEE/ASME Transactions on Mechatronics*, 22(4), pp.1850–1858.

Chivarov, N., Shivarov, S., Yovchev, K., Chikurtev, D., Shivarov, N., 2015. Intelligent modular service mobile robot ROBCO 12 for elderly and disabled persons care. *23rd International Conference on Robotics in Alpe-Adria-Danube Region, IEEE RAAD 2014 - Conference Proceedings*, (4).

Cho, B.-S., Moon, W., Seo, W.-J. and Baek, K.-R., 2011. A dead reckoning localization system for mobile robots using inertial sensors and wheel revolution encoding. *Journal of Mechanical Science and Technology*, 25(11), pp.2907–2917.

Choi, B.S., Lee, J.W., Lee, J.J. and Park, K.T., 2011. A Hierarchical Algorithm for Indoor Mobile Robot Localization Using RFID Sensor Fusion. *IEEE Transactions on Industrial Electronics*, 58(6), pp.2226–2235.

Chong, K.S.C.K.S. and Kleeman, L., 1997. Accurate odometry and error modelling for a mobile robot. *Proceedings of International Conference on Robotics and Automation*, 4(April), pp.2783–2788.

Chung, H., Ojeda, L. and Borenstein, J., 2001. Accurate Mobile Robot Dead-Reckoning with a Precision-Calibrated Fiber-OpticGyroscope. *IEEE Transactions on Robotics and Automation*, 17(1), pp.80–84.

Crisan, D. and Doucet, A., 2002. A survey of convergence results on particle filtering methods for practitioners. *IEEE Transactions on Signal Processing*, 50(3), pp.736–746.

D'Alfonso, L., Lucia, W., Muraca, P. and Pugliese, P., 2015. Mobile robot localization via EKF and UKF: A comparison based on real data. *Robotics and Autonomous Systems*, 74, pp.122–127.

Dang, Y., Wang, H. and Xu, W., 2016. Calibration of iRobot create using UMBmark. *2016 IEEE 14th International Workshop on Advanced Motion Control, AMC 2016*, pp.97–102.

Ericsson, J.E. and Eriksson, D., 2014. *Indoor Positioning and Localisation System with Sensor Fusion*. KTH Royal Institute of Technology.

Fang, H., Tian, N., Wang, Y., Zhou, M., Haile, M.A., 2018. Nonlinear Bayesian estimation: from Kalman filtering to a broader horizon. *IEEE/CAA Journal of Automatica Sinica*, 5(2), pp.401–417.

Feng, X., Jiang, J., Lin, P. and Wu, W.H., 2015. Radar target detection method based on particle filter theory under correlated non-Gaussian clutter backgrounds. *IET International Radar Conference 2015*. 2015 pp. 1–5.

Fung, M.L., Chen, M.Z.Q. and Chen, Y.H., 2017. Sensor Fusion : A Review of Methods and Applications. , pp.3853–3860.

Goel, P., Roumeliotis, S.I.S.I. and Sukhatme, G.S.G.S., 1999. Robust localization using relative and absolute position estimates. *Proceedings 1999 IEEE/RSJ International Conference on Intelligent Robots and Systems. Human and Environment Friendly Robots with High Intelligence and Emotional Quotients (Cat. No.99CH36289)*. 1999 pp. 1134–1140.

González, R. and Rodriguez, F., 2009. Comparative study of localization techniques for mobile robots based on indirect kalman filter. *Proc. of the IFR International Symposium on Robotics*. 2009 pp. 253–258.

Gordon, N.J., Salmond, D.J. and Smith, A.F.M., 1993. Novel approach to nonlinear/non-Gaussian Bayesian state estimation. *IEE Proceedings F - Radar and Signal Processing*. 1993 pp. 107–113.

Goronzy, G. and Hellbrueck, H., 2017. Weighted online calibration for odometry of mobile robots. *2017 IEEE International Conference on Communications Workshops, ICC Workshops 2017*, pp.1036–1042.

Guran, M., Fico, T., Chovancova, A., Duchon, F., Hubinsky, P., Dubravsky, J., 2015. Localization of iRobot create using inertial measuring unit. *23rd International Conference on Robotics in Alpe-Adria-Danube Region, IEEE RAAD 2014 - Conference Proceedings*, pp.1–7.

Hou, X., Yang, Y., Li, F. and Jing, Z., 2011. Kalman filter based on error state variables in SINS + GPS navigation application. *Information Science and Technology (ICIST), 2011 International Conference on*. 2011 pp. 770–773.

Huang, Z., Zhu, J., Yang, L., Xue, B., Wu, J., Zhao, Z., 2015. Accurate 3-D Position and Orientation Method for Indoor Mobile Robot Navigation Based on Photoelectric Scanning. , 64(9), pp.1–12.

Jaros, K., Witkowska, A. and Smierzchalski, R., 2017. Data fusion of GPS sensors using Particle Kalman Filter for ship dynamic positioning system. *2017 22nd International Conference on Methods and Models in Automation and Robotics (MMAR)*, pp.89–94.

Jeon, D., Choi, H. and Kim, J., 2016. UKF data fusion of odometry and magnetic sensor for a precise indoor localization system of an autonomous vehicle. *2016 13th International Conference on Ubiquitous Robots and Ambient Intelligence, URAI 2016*, pp.47–52.

Julier, S.J. and Uhlmann, J.K., 2004. Unscented filtering and nonlinear estimation. *Proceedings of the IEEE*, 92(3), pp.401–422.

Jung, C. and Chung, W., 2012. Accurate calibration of two wheel differential mobile robots by using experimental heading errors. *Proceedings - IEEE International Conference on Robotics and Automation*, pp.4533–4538.

Jung, C. and Chung, W., 2011. Design of test tracks for odometry calibration of wheeled mobile robots. *International Journal of Advanced Robotic Systems*, 8(4), pp.1–9.

Al Khatib, E.I., Jaradat, M.A., Abdel-Hafez, M. and Roigari, M., 2015. Multiple sensor fusion for mobile robot localization and navigation using the Extended Kalman Filter. *2015 10th International Symposium on Mechatronics and its Applications (ISMA)*, pp.1–5.

Kumari, B.L., Divya, V.Y. and Raju, K.P., 2015. Performance analysis of extended Kalman filter for single and multi target tracking. *2015 13th International Conference on Electromagnetic Interference and Compatibility (INCEMIC)*. 2015 pp. 202–204.

Kundu, A.S., Mazumder, O., Dhar, A., Lenka, P.K. & Bhaumik, S., 2017. Scanning Camera and Augmented Reality Based Localization of Omnidirectional Robot for Indoor Application. *Procedia Computer Science*, 105, pp.27–33.

Lee, S.-J., Tewolde, G., Lim, J. and Kwon, J., 2015. QR-code based Localization for Indoor Mobile Robot with validation using a 3D optical tracking instrument. *2015 IEEE International Conference on Advanced Intelligent Mechatronics (AIM)*, pp.965–970.

Lee, Y., 2015. A Reliable Range-free Indoor Localization Method for Mobile Robots. *2015 IEEE International Conference on Automation Science and Engineering (CASE)*, pp.720–727.

Leonard, J.J. and Durrant-Whyte, H.F., 1991. Mobile robot localization by tracking geometric beacons. *IEEE Transactions on Robotics and Automation*, 7(3), pp.376–382.

Li, K., Hu, B., Chang, L. and Li, Y., 2016. Comparison of direct navigation mode and indirect navigation mode for integrated SINS/GPS. *Transactions of the Institute of Measurement and Control*, 38(1), pp.3–13.

Lobo, A. et al., 2014. Localization and tracking of indoor mobile robot with beacons and dead reckoning sensors. *2014 IEEE Students' Conference on Electrical, Electronics and Computer Science, SCEECS 2014*, (1).

Luiz, D., Junior, T. and Todt, E., 2017. Rotational Odometry Calibration for Differential Robot Platforms.

Luo, R.C. and Chang, C.C., 2012. Multisensor fusion and integration: A review on approaches and its applications in mechatronics. *IEEE Transactions on Industrial Informatics*, 8(1), pp.49–60.

Lv, W., Kang, Y. and Qin, J., 2017. Indoor Localization for Skid-Steering Mobile Robot by Fusing Encoder, Gyroscope, and Magnetometer. *IEEE Transactions on Systems, Man, and Cybernetics: Systems*, pp.1–13.

Lynen, S., Achtelik, M.W., Weiss, S., Chli, M., Siegwart, R., 2013. A robust and modular multi-sensor fusion approach applied to MAV navigation. *2013 IEEE/RSJ International Conference on Intelligent Robots and Systems*. 2013 pp. 3923–3929.

Maddahi, Y., Maddahi, A. and Sepehri, N., 2013. Calibration of omnidirectional wheeled mobile robots: Method and experiments. *Robotica*, 31(6), pp.969–980.

Marín, L., Vallés, M., Soriano, Á., Valera, Á., Albertos, P., 2013. Multi Sensor Fusion Framework for Indoor-Outdoor Localization of Limited Resource Mobile Robots. *Sensors* , 13(10).

Maybeck, P.S., 1979. *Stochastic models, estimation, and control*, Academic Press, New York,USA.

Nasir, A.K. and Roth, H., 2012. *Pose estimation by multisensor data fusion of wheel encoders, gyroscope, accelerometer and electronic compass*, IFAC.

Nazemzadeh, P., Fontanelli, D., Macii, D. and Palopoli, L., 2017. Indoor localization of mobile robots through QR code detection and dead reckoning data fusion. *IEEE/ASME Transactions on Mechatronics*, 22(6), pp.2588–2599.

Ng, D.W.K., Soh, Y.W. and Goh, S.Y., 2014. Development of an autonomous BCI wheelchair. *IEEE SSCI 2014 - 2014 IEEE Symposium Series on Computational Intelligence - CIBCI 2014: 2014 IEEE Symposium on Computational Intelligence in Brain Computer Interfaces, Proceedings*. 2014 pp. 1–4.

Paliwal, K. and Basu, A., 1987. A speech enhancement method based on Kalman filtering. *ICASSP '87. IEEE International Conference on Acoustics, Speech, and Signal Processing*. 1987 pp. 177–180.

Panich, S. and Afzulpurkar, N., 2011. Mobile robot integrated with gyroscope by using IKF. *International Journal of Advanced Robotic Systems*, 8(2), pp.122–136.

Park, K., Chung, D., Chung, H. and Lee, J.G., 1996. Dead reckoning navigation of a mobile robot using an indirect Kalman filter. *Multisensor Fusion and Integration for Intelligent Systems, 1996. IEEE/SICE/RSJ International Conference on*. 1996 IEEE, Washington, DC, pp. 132–138.

Pelka, M. and Hellbrück, H., 2016. Introduction, discussion and evaluation of recursive Bayesian filters for linear and nonlinear filtering problems in indoor localization. *2016 International Conference on Indoor Positioning and Indoor Navigation, IPIN 2016*. 2016

Peter, G., Kiss, B. and Kovacs, G., 2016. Kalman filter based cooperative landmark localization in indoor environment for mobile robotsPeter, G., Kiss, B. and Kovacs, G., 2016. Kalman filter based cooperative landmark localization in indoor environment for mobile robots. 2016 IEEE International C. *2016 IEEE International Conference on Systems, Man, and Cybernetics (SMC)*, pp.001888–001893.

Péter, G., Kiss, B. and Kovács, G., 2016. Kalman filter based cooperative landmark localization in indoor environment for mobile robots. *2016 IEEE International Conference on Systems, Man, and Cybernetics (SMC)*. 2016 pp. 1888–1893.

Ruan, X., Li, Y. and Zhu, X., 2012. Kinematic parameter calibration of two-wheeled robot. *2012 IEEE International Conference on Mechatronics and Automation, ICMA 2012*, (2), pp.81–86.

Seongwoo Jang, Kyungjae Ahn, Jongseong Lee and Yeonsik Kang, 2015. A study on integration of particle filter and dead reckoning for efficient localization of automated guided vehicles. *2015 IEEE International Symposium on Robotics and Intelligent Sensors (IRIS)*, pp.81–86.

Sheijani, M.S., Gholami, A., Davari, N. and Emami, M., 2013. Implementation and performance comparison of indirect Kalman filtering approaches for AUV integrated navigation system using low cost IMU. *Electrical Engineering (ICEE), 2013 21st Iranian Conference on*, (Dvl), pp.1–6.

Skobeleva, A., Ugrinovskii, V. and Petersen, I., 2016. Extended Kalman Filter for indoor and outdoor localization of a wheeled mobile robot. *2016 Australian Control Conference (AuCC)*. 2016 pp. 212–216.

Tai, F.C., Tsai, C.C., Wang, X.C. and Chan, C.C., 2014. Decentralized EIF-based global localization using dead-Reckoning, KINECT and laser scanning for autonomous omnidirectional mobile robot. *2014 International Conference on Advanced Robotics and Intelligent Systems (ARIS)*. 2014 pp. 85–90.

Uddin, A.F.M.S., Uddin, M.J., Awal, M.A. and Islam, M.Z., 2017. Particle filter based moving object tracking with adaptive observation model. *2017 6th International Conference on Informatics, Electronics and Vision & 2017 7th International Symposium in Computational Medical and Health Technology (ICIEV-ISCMHT)*. 2017 pp. 1–6.

Umamageswari, A., Ignatious, J.J. and Vinodha, R., 2012. A Comparitive Study Of Kalman Filter, Extended Kalman Filter And Unscented Kalman Filter For Harmonic Analysis Of The Non-Stationary Signals. *International Journal of Scientific & Engineering Research*, 3(7), pp.1–9.

Utaminingrum, F., Fauzi, M.A., Wihandika, R.C., Adinugroho, S., Kurniawan, T.A., Syauqy, D.,Sari, Y.A., Adikara, P.P., 2017. Development of computer vision based obstacle detection and human tracking on smart wheelchair for disabled patient. *5th International Symposium on Computational and Business Intelligence, ISCBI 2017*, pp.1–5.

Wardana, A.A., Widyotriatmo, A., Janto, S. and Juliastuti, E., 2013. Experiment of a low cost computation particle filter for localization of an electric wheelchair. *Proceedings of 2013 International Conference on Robotics, Biomimetics, Intelligent Computational Systems, ROBIONETICS 2013*, (November), pp.155–159.

Won, P.S. h., Biglarbegian, M. and Melek, W., 2014. Development and performance comparison of extended Kalman filter and particle filter for self-reconfigurable mobile robots. *2014 IEEE Symposium on Robotic Intelligence in Informationally Structured Space (RiiSS)*. 2014 pp. 1–6.

Xuying, B., Xueliang, P. and Wenyan, G., 2017. Calibration of Systematic Errors for Wheeled Mobile Robots. , 1(9), pp.14–16.

Yang, S.W. and Wang, C.C., 2011. On Solving Mirror Reflection in LIDAR Sensing. *IEEE/ASME Transactions on Mechatronics*, 16(2), pp.255–265.

Yoon, S.W., Park, S. and Kim, J.S., 2015. Kalman Filter Sensor Fusion for Mecanum Wheeled Automated Guided Vehicle Localization. *Journal of Sensors*, 2015, pp.1–7.

Zaki, A.M., Arafa, O. and Amer, S.I., 2014. Microcontroller-based mobile robot positioning and obstacle avoidance. *Journal of Electrical Systems and Information Technology*, 1(1), pp.58–71.

Zhong, X., Zhou, Y. and Liu, H., 2017. Design and recognition of artificial landmarks for reliable indoor self-localization of mobile robots. *International Journal of Advanced Robotic Systems*, 14(1), pp.1–13.

Zhou, J. and Huang, L., 2011. Experimental study on sensor fusion to improve real time indoor localization of a mobile robot. *2011 IEEE 5th International Conference on Robotics, Automation and Mechatronics (RAM)*, pp.258–263.

APPENDIX A

EXPERIMENTAL RESULT OF PREVIOUS WORK

Figure A.1: The result of the two dominant systematic errors in both CCW and CW directions where (a) the error cancel off each other in one direction and (b) the error add up in another direction (Adapted from Borenstein and Feng, 1996)

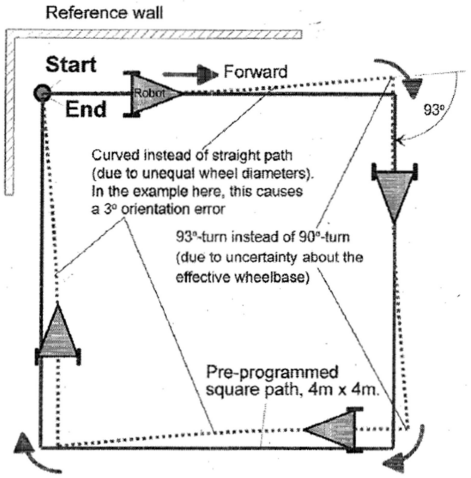

(a)

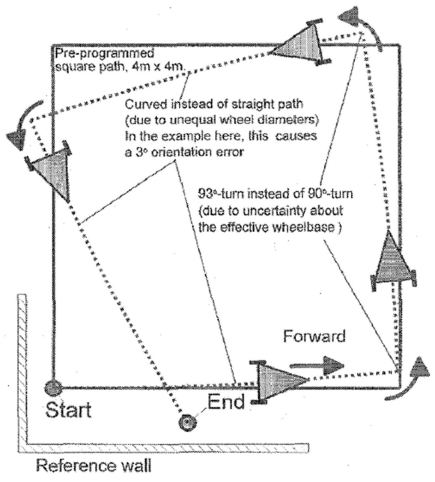

(b)